Check for updates

Received: 23 June 2022 | Revised: 9 April 2023 | Accepted: 4 June 2023

DOI: 10.1002/we.2845

RESEARCH ARTICLE

WILEY

Providing power reserve for secondary grid frequency regulation of offshore wind farms through yaw control

Younes Oudich[1] | Johan Gyselinck[2] | Frederik De Belie[3,4] | Michel Kinnaert[1]

[1]Control Engineering and System Analysis, Universite Libre de Bruxelles, Brussels, Belgium

[2]Bio- Electro- And Mechanical Systems, Universite Libre de Bruxelles, Brussels, Belgium

[3]Electromechanical, Systems and Metal Engineering, Ghent University, Ghent, Belgium

[4]Flanders Make, Ghent, Belgium

Correspondence
Younes Oudich, ULB - SAAS Avenue FD Roosevelt, 50-CP 165/55, 1050 Ixelles, Belgium.
Email: younes.oudich@ulb.be

Funding information
Federal Public Service Economy of Belgium, Grant/Award Number: PhairywinD; Belgian Energy Transition Fund

Abstract

The ability to significantly contribute to the frequency regulation and provide valuable ancillary services to the transmission system operator (TSO) is one of the present wind farm (WF) challenges, due to the limitations of wind speed forecasting and insufficient power reserve in certain operating conditions notably. In this work, the feasibility of WFs to participate in frequency restoration reserve (FRR) through yaw control is assessed. To this end, a distributed yaw optimization method is developed to evaluate the power gain achieved by yaw redirection based on wind turbine cooperation and compared with a greedy approach. The method relies on a static wake model whose parameters are estimated in a systematic way from simulation data generated with FAST.Farm. Through a case study based on a scaled version of the Belgian Mermaid offshore WF, it is demonstrated that the requirements of the TSO are fulfilled both in terms of response time and level of power reserve for most wind directions. The assessment is limited to wind speeds below the rated speed of the considered wind turbines.

KEYWORDS
frequency regulation, power reserve, wake effect, yaw optimization

1 | INTRODUCTION

With the increasing penetration of wind energy, wind farm (WF) operators have to participate in frequency regulation and support the traditional power plants in the electricity market.[1] Frequency regulation is generally subdivided into two control procedures. The first one is the primary frequency control, also known as frequency containment reserve (FCR); it requires fast reaction control loops to compensate for frequency variations. In the present case, the focus will be on frequency drops due to an excessive demand with respect to the generated power. The second one is the secondary frequency control, known as frequency restoration reserve (FRR); it can be achieved using slow supplementary control actions to bring back the frequency in the normal operational band. Such control procedures need a sufficient and predictable power reserve. The most common power reserve strategies for WFs are the *proportional delta control (PDC)* and the *constant delta control (CDC)*,[2] also known as curtailing (or derating) methods. The PDC consists in having a power reserve proportional to the available power in the entire wind speed range of the turbine characteristic, while the CDC aims at imposing a constant power reserve just in a specific wind speed range. These delta control strategies have been tested in the different wind speed operating regions of the wind turbine (WT), using the pitch and the torque controllers. Wang et al[3] have compared these methods, including their combination. The results show that either strategy on its own gives almost the same performance in terms of unused energy during FCR, while the combined one, although more complicated to implement, is more efficient.

This is an open access article under the terms of the Creative Commons Attribution-NonCommercial-NoDerivs License, which permits use and distribution in any medium, provided the original work is properly cited, the use is non-commercial and no modifications or adaptations are made.
© 2023 The Authors. *Wind Energy* published by John Wiley & Sons Ltd.

Many former works assessed the possibility for WTs to actively track power set-point commands using the previously presented curtailing methods, in order to participate in the utility grid. These works can be distinguished in two classes, one assessing these methods at a WT level, while the other one at a WF level. In the first category, Aho et al[4] combine curtailing with droop control to achieve primary and secondary frequency regulations. With the single WT simulated in OpenFAST,[5] and with a given power set-point to track as input, the assessed output power shows a good performance of the derated WT in tracking the power reference and thus assisting the grid frequency regulation. Van der Hoek et al[6] show the effects of the different curtailing methods on the lifetime of the WT components. Their conclusion indicates that all the methods reduce significantly fatigue loads over the lifetime. Looking at the second category, Deshpande and Peters[7] adjust the curtailing methods to prevent stall from derating the WTs and reduce the nonmonotonic response of the WT in case of a quick change of the input set-point. Such changes achieve derated power curves inducing lower mechanical loads due to avoided stall. Van Wingerden et al[8] propose a simple gain-scheduled proportional-integral feedback control at the WF level in order to correct the power reference of each turbine, which significantly improves the tracking behavior of the total output power of the WF.

Most of these primary and secondary frequency regulations are based on droop curves and curtailment like proportional delta and CDC. There is however one novel possible approach to power reserve which is not studied for FRR although its potential has been pointed out in the framework of WF power maximization. Indeed, it has been shown[9,10] that wake redirection of upstream WTs in a WF can induce a power production increase of the downstream turbines. This can result in a global power increase of the whole WF in comparison to a standard approach in which all turbines are facing the wind. Different control strategies to achieve wake redirection are possible,[9] such as yaw control, tilt control, and individual pitch control (IPC). The most common one is the yaw optimization control. Several works based on static wake models[10] demonstrate that the WF production increase varies from 3% to 18% thanks to the yaw steering method, depending on the wake model used and the WF layout, turbulence, and free wind speed. In these studies, a steady constant wind flow over the whole WF is assumed. Most of them validate their results either by comparison with measurements done in a wind tunnel or by comparison with a high-fidelity simulator, such as SOWFA,[11] which is computational fluid dynamics (CFD) based.

Wake redirection methods rely on a wake model in order to estimate the WF power while taking the wake effect into account. Several wake models have been assessed regarding their accuracy, implementation, and complexity,[12,13] from the most basic mathematical linear and static Jensen model to sophisticated ones based on high-fidelity simulators like SOWFA. For yaw optimization in real-time, the wake model should be sufficiently tractable computationally, while allowing a good approximation of the WF power in different configurations (wind speed and direction, and yaw angles). The first proposed far wake model is the N.O. Jensen wake model[14] which assumes a linearly expanding wake diameter with a constant wake deficit in the waked area. Brusca et al[13] compare this basic model to experimental data and to other simple wake models like the Larsen and Frandsen models. Measurements show that the wind speed in the waked area decreases gradually along the radius from the blade tips to the hub, contrary to the constant wake deficit of the Jensen model. To this end, Jensen[15] suggested a second and improved cosine-bell-shaped wake model, which was validated with experimental wake profiles data generated by Vermeulen et al.[16] To overcome the periodicity of the cosine function, Park and Law[17] propose an improved and more complex wake model based on the linear Jensen model, by adding a Gaussian-shaped factor instead of a cosine-bell one and by taking the wake deflection into account. The model was validated after fitting its parameters to the wind speed profiles downstream a WT obtained by SOWFA simulations.[18,19] However, the objective is to estimate not only the wind profile but also the produced power. The latter was considered in reference,[20] but no systematic parameter estimation method was reported.

The goal of this article is to assess the possibility to achieve FRR services thanks to wake redirection. More precisely, we evaluate whether the additional power available via wake redirection by yaw control can be considered as an adequate reserve for FRR, given the requirements in terms of available power and timing set by the Belgian TSO. The contributions of the present work can be summarized as follows. A systematic approach is proposed to fit the parameters of the static wake model for power estimation including the Gaussian wake deficit, which was not considered previously.[20] Next, a distributed yaw optimization algorithm is proposed and compared with existing methods in terms of computing time.[10] Finally, it is demonstrated that yaw redirection can be used for FRR because it fulfils TSO requirements both in terms of response time and amount of power reserve in a realistic offshore WF test case (Belgian Mermaid offshore WF[21]). However, the yawing transient should be properly accounted for when designing the FRR power reference.

The paper is organized as follows. In Section 2, the frequency control requirements of the Belgian TSO are presented. In Section 3, the wake model used for yaw optimization is described and the estimation of its parameters is addressed. In Section 4, different methods for yaw optimization are described and compared, including the suggested one. Section 5 is dedicated to a case study based on a scaled version of the Mermaid WF. Finally, some concluding remarks are provided in Section 6.

2 | FCR AND FRR SPECIFICATIONS BY THE BELGIAN TSO

Each TSO has its own frequency control specifications. Since this work is part of the Belgian PhairywinD project,[22] the specifications of the Belgian TSO, named Elia, are considered. Although the focus of our work is on FRR, we present requirements for both FCR and FRR as they are linked.

10991824, 2023, 8, Downloaded from https://onlinelibrary.wiley.com/doi/10.1002/we.2845 by EVIDENCE AID - BELGIUM, Wiley Online Library on [03/10/2023]. See the Terms and Conditions (https://onlinelibrary.wiley.com/terms-and-conditions) on Wiley Online Library for rules of use; OA articles are governed by the applicable Creative Commons License

2.1 | FCR requirements

The requirements for becoming a provider of primary frequency control are illustrated in Figure 1.[23] In the normal operating band (the frequency deviation $|df| < 200$ mHz), the measured grid frequency (blue line) must be within the range 50 Hz ± 10 mHz (orange dashed lines). Otherwise, FCR providers must deliver their power reserve bid until $|df|$ is back in the acceptable range. In addition, if the FCR providing source is limited in reserve, then it must deliver its FCR bid for at least 15 min.

2.2 | FRR requirements

In Elia's domain, the FRR is a 1-day ahead market, where each provider has to give its forecasted power bid while accounting for FRR specifications.[24,25] For WF operators, the maximum power production should be forecasted 1 day ahead with 15 min resolution. The operators can also make a FRR power bid (minimum 1 MW) that should be delivered 100% at any time within the coming day, for 15 min and after 15 min of preparation and ramp-up.

Once the power reserve for FRR is determined, the power reference delivered to Elia must be evaluated. Figure 2 gives an example for the possibility to deliver FRR while following the reference set-points for a WF. The total available power at the present time is sketched by the green line, while it has been forecasted 1 day ahead to be the blue dashed line (60 MW at t_0). Based on the forecasting uncertainties, the WF operator a priori determines a power reference considering its power reserve bid. For instance, if it is forecasted that there is a 99% probability that the WF production will exceed 50 MW from t_0 to t_0+15 min (orange dashed line) and the power reserve bid decided by the operator is 5 MW (green-yellow dashed area), then the maximum power reference the producer imposes can be 45 MW (from t_0 to t_0+15 min). Once the power reference is set by the WF operator, Elia sends back the set-points to follow every 4–5 s.

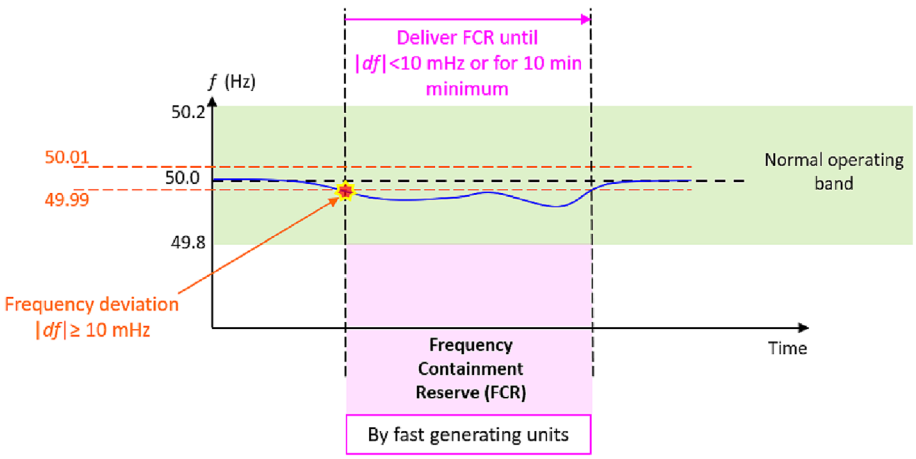

FIGURE 1 Frequency containment reserve (FCR) delivery in the normal operating band.

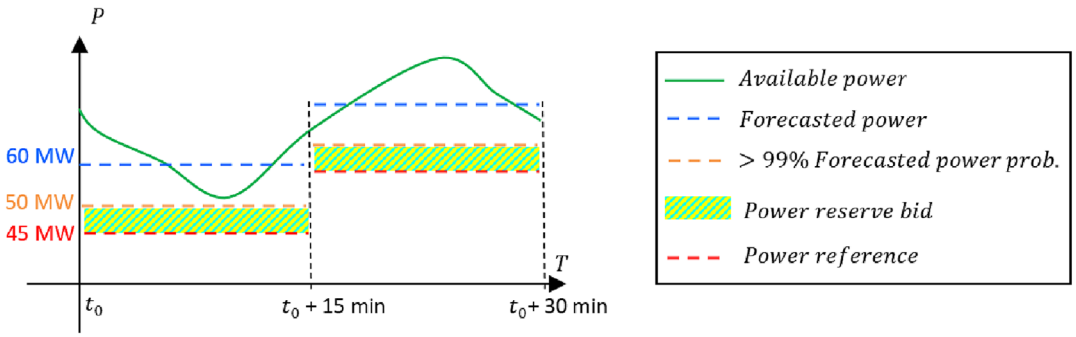

FIGURE 2 Example of a wind farm (WF) provider participating in frequency restoration reserve (FRR) delivery.

10991824, 2023, 8, Downloaded from https://onlinelibrary.wiley.com/doi/10.1002/we.2845 by EVIDENCE AID - BELGIUM, Wiley Online Library on [03/10/2023]. See the Terms and Conditions (https://onlinelibrary.wiley.com/terms-and-conditions) on Wiley Online Library for rules of use; OA articles are governed by the applicable Creative Commons License

2.3 | Delivery of FCR and FRR in case of a frequency deviation due to a faulty generator

When a fault in the grid happens at $t = t_0$ and causes the grid frequency to deviate beyond the normal operating band ($|df|$>200 mHz), FCR and FRR should be delivered as soon as possible, respecting the maximum time delays given in Figure 3. In the worst-case scenario, the FCR has 30 s from t_0 to ramp-up to its full capacity, delivering it for 15 min. During this period, FRR has a 30 s time response delay maximum from t0, followed by 7.5 min of preparation and another 7.5 min to ramp-up to its full capacity that should be delivered for 15 min. Focusing on the time scale requirements, FRR can be achieved by slow supplementary units, delivering their full capacity after several minutes.

As stated in Section 1, the aim of the present work is to assess the possibility to provide FRR services through yaw control, given the presented requirements in terms of timing and available power set by Elia. To evaluate the power reserve thanks to the yaw steering method, the power produced by each WT in the park must be reliably estimated. As wake can have a significant impact,[9,10] its influence on the produced power is addressed in the next section.

3 | WAKE EFFECT MODEL

The wake deflection method is based on a wake model. Therefore, and as stated in Section 1, we consider a Gaussian-shaped Jensen wake model, inspired from previous works.[18,20]

3.1 | Gaussian wake effect model

Let us consider the j^{th} WT within a WF, subject to the free wind speed U_0 in X direction, with a yaw angle γ_j as depicted in the top view in Figure 4. The downstream wind speed u at a distance x is computed as follows:

$$u(x,r,a_j,\gamma_j) = (1+\delta u(x,r,a_j,\gamma_j))U_0, \tag{1}$$

with a_j the induction factor, r the radial distance from the center of the wake, and δu the wake deficit given by the following:

$$\delta u(x,r,a_j,\gamma_j) = \begin{cases} -2a_j \cos(\mu\gamma_j)\left(\frac{R}{R+kx}\right)^2 \exp\left(-\left(\frac{r}{R+kx}\right)^2\right) & ;x>0 \\ 0 & ;x\le 0. \end{cases} \tag{2}$$

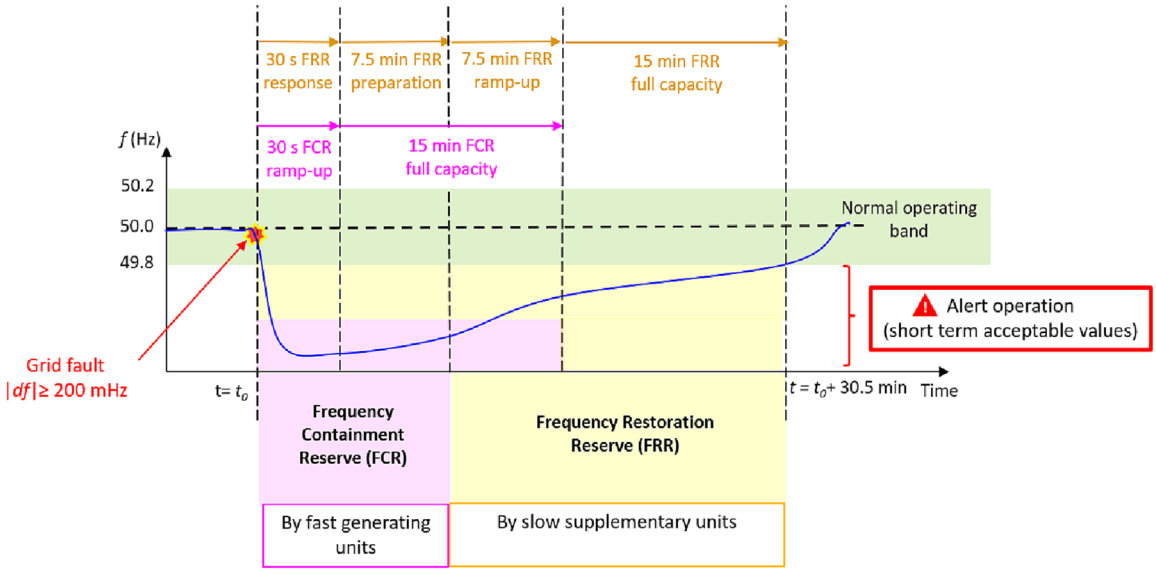

FIGURE 3 Frequency restoration reserve (FCR) and frequency restoration reserve (FRR) delivery in the alert operation.

10991824, 2023, 8, Downloaded from https://onlinelibrary.wiley.com/doi/10.1002/we.2845 by EVIDENCE AID - BELGIUM, Wiley Online Library on [03/10/2023]. See the Terms and Conditions (https://onlinelibrary.wiley.com/terms-and-conditions) on Wiley Online Library for rules of use; OA articles are governed by the applicable Creative Commons License

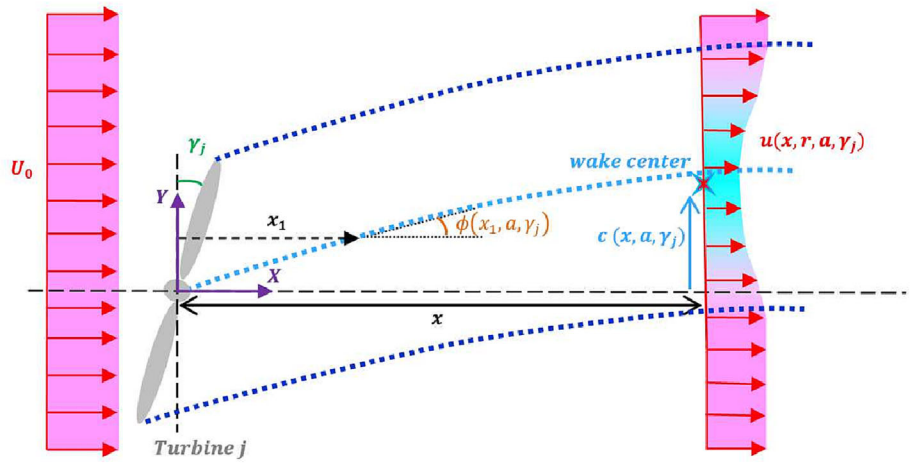

FIGURE 4 The wake effect between the dark blue dashed lines, representing its edges, is induced by turbine j at distance x. The yaw angle of turbine j is γ_j. The blue-sky dashed line represents the wake center deviation c.

In (2), $R = \frac{D}{2}$ is the radius of the WT rotor, and μ and k are constant parameters defining the effect of the yaw angle on the wake deficit amplitude and the wake expansion, respectively. The condition ($x > 0$) ensures the wake to be downstream the WT j. The area subject to wake effect of turbine j is located between the dark blue dashed lines in Figure 4. The wake center c (blue-sky dashed line) is determined by the following:

$$c(x, a_j, \gamma_j) = \int_0^x \tan\left(\phi(s, a_j, \gamma_j)\right) ds - \tau(x), \tag{3}$$

where ϕ and τ are the angle of the wake center line from the X direction due to the yaw angle and the wake deflection due to the rotation of the rotor, respectively. Both are defined as follows:

$$\phi(x, a_j, \gamma_j) \approx \frac{2a_j(1 - a_j)\cos^2\gamma_j \sin\gamma_j}{\left(1 + \frac{k_d x}{R}\right)^2}, \tag{4}$$

$$\tau(x) = a_d + b_d x, \tag{5}$$

where k_d, a_d, and b_d are constant values to be determined.

Introducing a turbine i downstream from turbine j as depicted in Figure 5, the effective wake deficit affecting WTi, $\delta\bar{u}_{ij}$, is computed by integrating the wake deficit generated by the first turbine on the rotor plane of the second one:

$$\delta\bar{u}_{ij}(x_{ij}, a_j, \gamma_j) = \frac{1}{\pi R^2} \int_0^{2\pi} \int_0^R \delta u\left(x_{ij}, r(r', \theta', a_j, \gamma_j), a_j, \gamma_j\right) r' dr' d\theta', \tag{6}$$

where x_{ij} is the distance between WTj and WTi along the X axis, r' and θ' are the polar coordinates on the rotor plane of turbine i, and r is the radial distance from the center wake to a point with polar coordinates (r', θ') given by the following:

$$r(r', \theta', a_j, \gamma_j) = \sqrt{\left(y_{ij} - c(x_{ij}, a_j, \gamma_j) + r'\cos\ (\theta')\right)^2 + \left(r'\sin\ (\theta')\right)^2}. \tag{7}$$

Once the effective wake deficits of all upstream WTs j on turbine i are calculated, the overall wake deficit taking into account the wake interaction is set as follows, based on the widely used method of the conservation of kinetic energy proposed by Katic et al.[14]:

10991824, 2023, 8, Downloaded from https://onlinelibrary.wiley.com/doi/10.1002/we.2845 by EVIDENCE AID - BELGIUM, Wiley Online Library on [03/10/2023]. See the Terms and Conditions (https://onlinelibrary.wiley.com/terms-and-conditions) on Wiley Online Library for rules of use; OA articles are governed by the applicable Creative Commons License

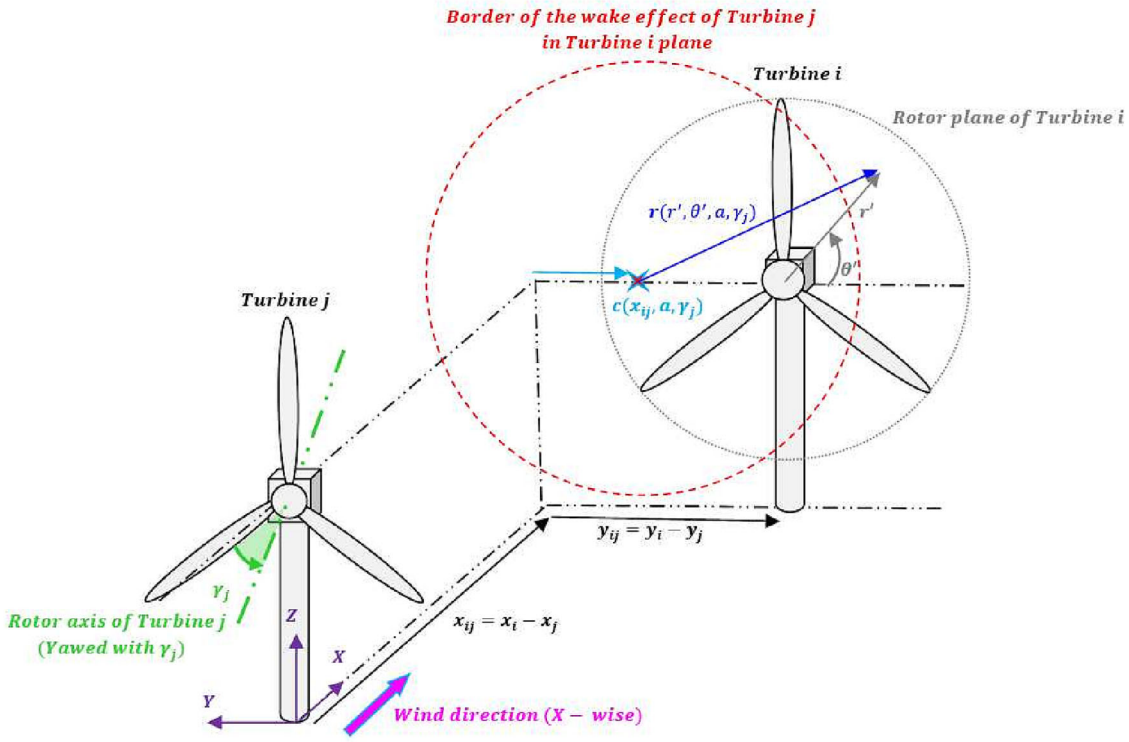

FIGURE 5 The 3D view of the different parameters in the described wake model.

$$\delta\hat{u}_i = \sqrt{\sum_{j \neq i} \delta\bar{u}_{ij}^2 (x_{ij}, a_j, \gamma_j)}. \tag{8}$$

Finally, the power generated by the waked turbine i is as follows:

$$P_i(\lambda_i, \beta_i, \gamma_i, U_0) = \frac{1}{2}\eta\rho\pi R^2 C_p(\lambda_i, \beta_i)((1 - \delta\hat{u}_i)U_0)^3 \cos^3\gamma_i, \tag{9}$$

where $\eta = 9.78 \cdot 10^{-1}$ the power loss factor representing the mechanical losses and $C_p(\lambda_i, \beta_i)$ is the power coefficient that depends on the tip-speed ratio λ_i at the effective wind speed upstream WT i, $(1 - \delta\hat{u}_i)U_0$, and the pitch angle β_i. Note that the power coefficient of the cosine in 9 is chosen to be 3, meaning that only the normal flow to the disk is considered. This is in line with the assumptions behind the FAST.Farm software that will be used for generating the synthetic data exploited for parameter estimation. Otherwise, this coefficient can have a lower value.[26]

This wake model is known to be valid for far wake, namely, from a distance beyond approximately three times the rotor diameter downstream a turbine ($x_{ij} \geq 3D$).[27,28] The wake model has been validated in previous works[18,19] for turbines operating in the second region, namely, the maximum power point tracking (MPPT) zone. In the present case, the 5MW-NREL Horizontal Axis Wind Turbine (HAWT)[29] is considered, and some of its characteristics are given in Table 1. Its MPPT region corresponds to wind speeds in the interval $U_0 \in [7.85; 10.24]$ m/s, ensuring the induction factor a to be equal to its optimal value $\frac{1}{3}$. In this cases, the power coefficient $C_p(\lambda_{opt}, \beta_{opt})$ is equal to its maximum, namely, 0.48 in the present case,[29] corresponding to the optimal tip speed ratio $\lambda_{opt} = 7.55$ and optimal pitch angle $\beta_{opt} = 0^\circ$. Finally, similar to studies on power optimization, the wind turbulence and time-dependency are not considered here for sake of simplicity of the model.[18–20] The impact of the latter hypothesis will be evaluated in Section 5.2.

3.2 | Parameter estimation of the model

In the absence of actual WF data, we resort here to a WF simulator to generate data allowing to estimate the parameters of the wake model. In this research paper, the open-source software FAST.Farm has been chosen for its inflow model accuracy and for its computational speed.

10991824, 2023, 8, Downloaded from https://onlinelibrary.wiley.com/doi/10.1002/we.2845 by EVIDENCE AID - BELGIUM, Wiley Online Library on [03/10/2023]. See the Terms and Conditions (https://onlinelibrary.wiley.com/terms-and-conditions) on Wiley Online Library for rules of use; OA articles are governed by the applicable Creative Commons License

TABLE 1 Some characteristics of the 5MW-NREL HAWT.[29]

Parameter	Value
Rated power	5 MW
Number of blades	3
Rotor diameter (m)	126
Hub height (m)	90
Cut-in, rated, and cut-out wind speeds, respectively (m/s)	3 & 11.4 & 25
Cut-in and rated rotor speed, respectively (rpm)	6.9 & 12.1
Maximum yaw rate (°/s)	0.3

TABLE 2 Some advantages and limitations of FAST.Farm according to Jonkman et al.[32]

FAST.Farm predicts well the following:	FAST.Farm is limited when it comes to the following:
- Output data: powers, torques, generator speeds, loads, and more of individual WTs within a WF.	- Near wake effects (e.g. vortex breakdown).
- Time series of wake meandering.	- Wake-added turbulence having low ambient TI.
- Far wake deficit advection, evolution, and merging.	- Wake-induced boundary layers and flow speed-up around the WTs.
- Statistical distributions of the output data.	- Curled wakes under skewed-flow conditions.
	- Wake asymmetry.

Abbreviations: TI, turbulence intensities; WF, wind farm; WT, wind turbine.

Therefore, the following section gives a brief introduction to the FAST.Farm simulator used for data generation. Based on this tool, the problem of estimating the model parameters is addressed.

3.2.1 | FAST.Farm simulator

FAST.Farm[30] is a midfidelity WF simulator developed by the National Renewable Energy Laboratory (NREL), aiming at solving the nonlinear aero-hydro-servo-elastic dynamics of each WT, within the atmospheric boundary layer (ABL). It is able to account for several physical phenomena, such as the effects of local inflow skew, shear, turbulence, tower flow disturbances, and structural motion. Moreover, FAST.Farm considers additional models, such as wake deficits, advection, deflections, meandering, and merging to represent the different physical phenomena in the WF domain.

The rotor aerodynamics in FAST.Farm are computed via OpenFAST,[5] which uses the blade-element momentum theory (BEM), including some advanced corrections such as the Prandtl tip-loss, Prandtl hub-loss, Pitt and Peters skewed-wake, and the Glauert's empirical correction. The wake dynamics (in FAST.Farm) are modeled using the thin shear-layer approximation of the Reynolds-averaged Navier–Stokes equations.[30] The latter approach induces the wake deficit to be valid only in the far wake. However, because the wake deficit evolution starts at the rotor plane of the WT, a near-wake correction was added which also improves accuracy of the far wake.[30] The wake model of FAST.Farm has numerous parameters to tune, which can be specified by the user. These parameters were calibrated using SOWFA, based on a single 5MW-NREL WT, under nine scenarios for various atmospheric stability conditions and various values for turbulence intensities (TI), shear exponents, and yaw errors.[31] Thereafter, FAST.Farm has been validated using six other scenarios with different values for the number of turbines mean wind speeds, TI, shear exponents, and yaw errors.[32] SOWFA is a high-fidelity WF simulator also developed by NREL. It is based on the large eddy simulation (LES) turbulence model and the actuator-line method to describe the physics within a WF. SOWFA requires up to 1 billion mesh cells, which leads to a heavy computation complexity and thus very time-consuming simulations. Consequently, NREL developed FAST.Farm to perform simulations with a reasonable compromise between computing time and quality of the generated synthetic data. Some of the advantages and limitations of FAST.Farm can be found in the work of Jonkman et al[32] and are summed up in Table 2.

3.2.2 | Estimation of wake model parameters

The FAST.Farm simulator is used to simulate an arrangement of two turbines ($N_T = 2$) with relative positions depicted in Figure 6. For each steady wind speed $U_0 \in \{8,9,10\}$ m/s and for each position of the upstream WT (Turbine 1) on the X-Y axes indicated in Figure 6

10991824, 2023, 8, Downloaded from https://onlinelibrary.wiley.com/doi/10.1002/we.2845 by EVIDENCE AID - BELGIUM, Wiley Online Library on [03/10/2023]. See the Terms and Conditions (https://onlinelibrary.wiley.com/terms-and-conditions) on Wiley Online Library for rules of use; OA articles are governed by the applicable Creative Commons License

$(\frac{X}{D}, \frac{Y}{D}) \in \{4,5,6,7,8\} \times \{-1, -0.5,0,0.5,1\}$, Turbine 1 is yawed with an angle γ_1 from -30° to 30° with 5° increment. The steady wind flow follows a power law formula, given by

$$v_x = U_0 \left(\frac{z}{z_{ref}}\right)^{\Psi}; v_y = 0; v_z = 0, \tag{10}$$

where z_{ref} is the reference height and Ψ is the power law exponent. The considered parameters in the present study are z_{ref} =90 m, which represents the hub-height of the WT, and Ψ =0.2. Turbine 2 is always fixed in space and facing the wind direction ($\gamma_2 = 0^\circ$). Consequently, there are $N_{sim} = N_X \cdot N_Y \cdot N_{U_0} \cdot N_{\gamma_1} = 975$ simulations, with $N_X = 5$ and $N_Y = 5$ the number of X and Y positions, respectively, $N_{U_0} = 3$ the number of free wind speeds, and $N_{\gamma_1} = 13$ the number of yaw angles. Each simulation was run for 20 min which is sufficient to reach steady state. This provided us with the produced power of Turbines 1 and 2 as a function of the wind speed, of the positions, and the yaw angle of Turbine 1.

Letting $\zeta = [k, \mu, k_d, a_d, b_d]^T$ denote the vector of the parameters to be estimated, the following optimization problem is solved in order to estimate the model parameters:

$$\begin{aligned} \zeta^* = \arg\min_{\zeta} & \sqrt{\frac{1}{N_T \cdot N_{sim}} \sum_{(X_n,Y_m)}^{N_X \times N_Y} \sum_{i=1}^{N_{U_0}} \sum_{k=1}^{N_{\gamma_1}} \sum_{j=1}^{N_T} \left(P_{model,j}^{(X_n,Y_m)}(\gamma_{1,k}; U_{0,i}) - P_{FF,j}^{(X_n,Y_m)}(\gamma_{1,k}; U_{0,i}) \right)^2} \\ \text{s.t.} \quad & 0 < \zeta(1) \le 0.1; 0 < \zeta(2) \le 3; 0 < \zeta(3) \le 1; 0 \le \zeta(4) \le 10; 0 \le \zeta(5) \le 0.1, \end{aligned} \tag{11}$$

where $P_{model,j}^{(X_n,Y_m)}(\gamma_{1,k}; U_{0,i})$ and $P_{FF,j}^{(X_n,Y_m)}(\gamma_{1,k}; U_{0,i})$ are the output powers of turbine j at the free wind speed $U_{0,i}$ of the model and FAST.Farm, respectively, having the upstream turbine yawed by $\gamma_{1,k}$ and located at (X_n, Y_m). The upper bounds on the parameter values are chosen to be 10 times greater than their nominal value found in the literature, except for μ. The upper bound for the latter is set to 3 to ensure that the contribution of the cosine in (2) is always positive in the considered range of γ_1, namely, $[-30^\circ, 30^\circ]$.

The optimization problem is solved numerically by resorting to the interior-point method (via MATLAB and the built-in function `fmincon`[33]). A multistart approach is used to deal with local optima. Besides the initial value for ζ taken from the literature, 99 other values are selected at random, and the parameter estimation problem is solved for each of these sets of values. The algorithm is observed to converge to the same solution $\zeta^* = [0.0316, 2.41, 0.209, 0.00, 0.00]^T$ in all cases. Table 3 gives a comparison between the obtained optimal parameters and some of the values reported in the literature. Due to the difference in the wake models and the tuning methods, not all parameters are available in every work. However, note that the wake expansion coefficient k is close to most of the reported values, especially to the one from Pena et al,[34] that assess this wake expansion by comparing it to simulations and experimental data. Moreover, a_d and b_d are zero here, because FAST.Farm does not consider the wake redirection due to the rotation of the rotor. The validation of the wake model will be discussed in Section 5.2.

4 | PRESENTATION OF YAW OPTIMIZATION ALGORITHMS

Recall from Section 1 that the goal of this work is to view the difference between the WF maximum available power, through yaw steering method, and the classical configuration, where all the WTs face the wind direction, as a possible power reserve that may be used for FRR. Now

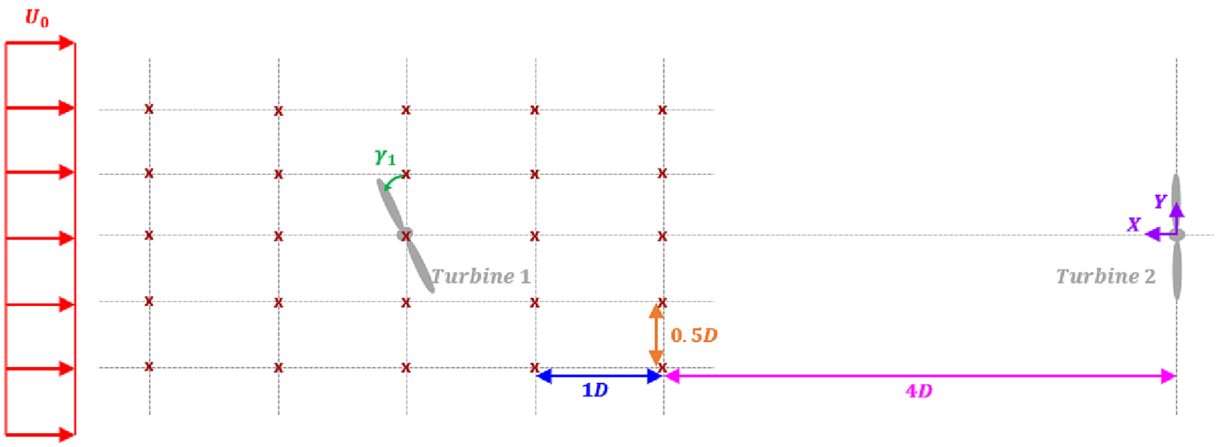

FIGURE 6 Sketch showing a top view of the simulation setup with the different positions of Turbine 1 in space.

10991824, 2023, 8, Downloaded from https://onlinelibrary.wiley.com/doi/10.1002/we.2845 by EVIDENCE AID - BELGIUM, Wiley Online Library on [03/10/2023]. See the Terms and Conditions (https://onlinelibrary.wiley.com/terms-and-conditions) on Wiley Online Library for rules of use; OA articles are governed by the applicable Creative Commons License

TABLE 3 Wake model parameters comparison with some literature values.

Model parameters	Present work	Park et al.[18]	Pena et al.[34]	Gebraad et al.[20]
k	0.031	0.031	0.038	0.065
μ	2.41	1.54	-	-
k_d	0.209	1.122	-	0.15
a_d	0	-	-	−4.5
b_d	0	-	-	−0.01

that a wake model is available, an efficient and fast yaw optimization algorithm can be built in order to assess the potential power gain through wake steering. Yaw optimization algorithms can be classified into two categories:

- *Centralized optimization algorithms*: Optimize the yaw angles of the individual WTs in order to maximize the whole wind park power, taking into account the wake effects. This can be done by classical optimization methods such as the interior-point method or by random search algorithms. The latter optimize the individual yaw angles by selecting a random set of yaw angles at each iteration and comparing the new WF power with the highest one found in the previous iterations. These types of algorithms have the advantages to be accurate and simple to implement. Meanwhile, they become time-consuming as the size of the WF grows, since finding the optimum becomes harder with the increase of the number of possible yaw angles and the aerodynamic interactions within the WF.[19,20,35]
- *Distributed optimization algorithms*: Consider the WF as a directed network, where the turbines are the nodes and the aerodynamic interactions are the edges. The goal is to split the WF into subsets and distribute the optimization algorithm among the subsets. By maximizing their power output, the overall WF power is maximized. These algorithms perform the optimization much faster than the centralized ones, but they are less accurate and more complex to implement.[19,36]

In this work, a new network distributed algorithm inspired from Annoni et al[36] will be presented. It will be shown that it outperforms three classical centralized algorithms in terms of computing time, while being similarly accurate and simple to implement. The optimized yaw angles for power maximization are found solving the following constrained problem:

$$\begin{aligned} \Gamma^* &= \arg\min_{\Gamma}\left(1-\frac{\sum_{j=1}^{N_T}P_j}{N_T P_{nom}}\right) \\ \text{s.t.}\quad -30^\circ &\le \Gamma(j) \le 30^\circ \qquad \forall j = 1,2,\ldots,N_T, \end{aligned} \tag{12}$$

with Γ the yaw angle vector of the individual turbines ($\Gamma(j)=\gamma_j$), N_T the total number of WTs, P_j the power of the individual turbine j, and P_{nom} the nominal power of each WT (still 5 MW). For the sake of completeness, three centralized algorithms are briefly described hereafter, before elaborating on our proposed distributed algorithm.

1. **Interior-point (IP) method (centralized optimization algorithm)**: As presented in Section 3.2.2, this classical optimization method aims at finding a local minimum of a constrained nonlinear multivariable objective function, starting from an initial guess point. This optimization algorithm is implemented within the `fmincon` MATLAB function.[33]
2. **Random search (RS) algorithm (centralized optimization algorithm)**: The RS algorithm, proposed by Kuo et al,[35] is based on a random incremental yaw angle selected in a range that tightens as the iteration number n grows. The algorithm starts by computing the output power of the WF where all the WTs are facing the wind direction (wind direction perpendicular to the WTs rotor planes) and saves this configuration as the best one. Next, this configuration is changed by yawing a percentage F of turbines within the WF by adding yaw angles randomly selected in the range $[-\beta_n^{\vec{?}},\beta_n^{\vec{?}}]$. If the new WF power is higher, then the best known configuration is updated accordingly. This process is repeated until the total number of iterations is reached, leading to a sufficient convergence toward the optimal solution of problem (12).
   The choice of β_n is dependent on the iteration number n as follows:

$$\beta_n = 7e^{-\kappa n/N_{iter}} + m \quad [^\circ], \tag{13}$$

   where κ and m are constant parameters and N_{iter} is the total number of iterations. This choice of β_n is made with the aim of having a wide range of yaw angles at the beginning of the algorithm and gradually tightening it as the iteration number grows, to refine output results. Kuo

10991824, 2023, 8, Downloaded from https://onlinelibrary.wiley.com/doi/10.1002/we.2845 by EVIDENCE AID - BELGIUM, Wiley Online Library on [03/10/2023]. See the Terms and Conditions (https://onlinelibrary.wiley.com/terms-and-conditions) on Wiley Online Library for rules of use; OA articles are governed by the applicable Creative Commons License

et al[35] propose to set $N_{iter} = 1000, \kappa = 5, m = 4°$, and $F = 5.1\%$ for large WFs of around 30 WTs, which fits to our study case that will be presented later on.

3. **Serial-refine (SR) algorithm (centralized optimization algorithm)**: The SR algorithm, proposed by Fleming et al,[37] proceeds in three main steps for finding the yaw angles achieving power maximization. The first step consists in sorting the WTs from the most upstream to the most downstream one, excluding the latter from the optimization process, because it is already optimized at zero yaw angle. The second step, called "Serial pass", tries N_{yaws} yaw angles equally spaced within a large range, for each turbine and compares the WF power to the best configuration so far. The resulting optimized yaw angles are saved in a vector Y_{opt}. The second pass (third step), called the "Refine pass", adds offset yaw angles to Y_{opt}, also equally spaced by N_{yaws} within a smaller range, for each turbine and compares once again the resulting WF power to the best configuration so far. Default values suggested by Fleming et al[37] for the large range are $[-30^{\circ}, 30^{\circ}]$ and for the small range are $[-7.5^{\circ}, 7.5^{\circ}]$. Besides, $N_{yaws} = 5$ is considered in this reference, in which case the serial pass uses the yaw angles $\{-30^{\circ}, -15^{\circ}, 0^{\circ}, 15^{\circ}, 30^{\circ}\}$ for each turbine, and the offset that is added in the refine pass belongs to the set $\{-7.5^{\circ}, -3.75^{\circ}, 0^{\circ}, 3.75^{\circ}, 7.5^{\circ}\}$. This yaw optimization algorithm is thus based on discrete angles depending on the variable N_{yaws}.
4. **Recursive neighbor function (RNF) algorithm (distributed optimization algorithm)**: As Annoni et al[36] state, a WF can be seen as a directed network since the wake of a WT only affects the downstream ones. The aim is to divide the WF into subsets, then maximize their power output. Inspired from the above reference, a new edge criterion is proposed in this research to choose the WF subsets.

   First, all the turbines are sorted within the wind direction of the free wind speed U_0, from most downstream to most upstream. The X-axis is along the wind direction from now on, as it can be seen in Figure 7. Starting from one of the most downstream turbines i, the edge criterion δ_{ij} between the turbines i and j is evaluated, as shown in Figure 7A. The criterion is a Boolean function of two parameters x_{ij} and σ_{ij}. A downstream turbine i is considered waked by turbine j ($\delta_{ij} = True$) if:

   (a) The inner distance x_{ij} as sketched in Figure 7B is less than $10D$ and greater than $3D$. $x_{ij} \leq 10D$ means that the turbine j must be located within $10D$, assuming the recovery of the wake effect behind $10D$. $x_{ij} \geq 3D$ is the minimum distance between two turbines in all directions considering our study case that will be presented in the next section. The impact of the assumption on the wake recovery behind $10D$ will be discussed later in Section 5.3.

   (b) Focusing on Figure 7B and thanks to the wake expansion parameter k found in Section 3.2.2, the wake diameter D_w at x_{ij} is given by the following:

$$D_w = D + 2kx_{ij}. \tag{14}$$

   Besides, the distance between the closest blade tip of turbine i and the rotor axis of turbine j is computed as follows:

$$\sigma_{ij} = \min\left(\left|y_i - \frac{D}{2} - y_j\right|; \left|y_i + \frac{D}{2} - y_j\right|\right). \tag{15}$$

   Finally, if $\sigma_{ij} \leq \frac{D_w}{2}$, then turbine i is affected by the wake of turbine j.

Based on the previous points, the Boolean function δ_{ij} can be defined as follows:

$$\delta_{ij} = \Lambda(x_{ij}, \sigma_{ij}) = \begin{cases} True & ;\textbf{if } (3D \leq x_{ij} \leq 10D) \textit{ and } \left(\sigma_{i,j} \leq \frac{D_w}{2}\right), \\ False & ;\textbf{else}. \end{cases} \tag{16}$$

When $\delta_{ij} = True$, turbines i and j are considered to be neighbors.

With the goal of finding the subsets of turbines that are mutually interacting through wake, it is crucial to determine not only the neighbors of a WT but also the neighbors of the neighbors. To do so, the RNF algorithm is proposed as given in Algorithm 1. As stated previously, the set of the WTs, Ω, must be descent sorted in the wind direction. By starting from the most downstream turbine i, a subset Ω_i is created containing only the selected turbine to begin with, and it is omitted from Ω to avoid being taken again later. Then, by computing the vector Δ of elements δ_{ij} for all the $j \in \Omega$, the elements where δ_{ij} is $True$ are filtered. If there are no upstream neighbors, then Ω_i is returned. Otherwise, for each of the neighbors found, the RNF algorithm is called again taking a neighbor j as the selected turbine and Ω as the WF set. The function calls itself recursively until no neighbor is found and a subset Ω_j is returned. This subset is added to Ω_i and omitted from Ω to avoid retaking the same set of turbines later on.

Once the subsets are built, the problem of yaw optimization for power maximization is defined for each subset by the same objective function as (12). The overall power of the WF is thus computed by the sum of the maximized powers from the subsets.

10991824, 2023, 8, Downloaded from https://onlinelibrary.wiley.com/doi/10.1002/we.2845 by EVIDENCE AID - BELGIUM, Wiley Online Library on [03/10/2023]. See the Terms and Conditions (https://onlinelibrary.wiley.com/terms-and-conditions) on Wiley Online Library for rules of use; OA articles are governed by the applicable Creative Commons License

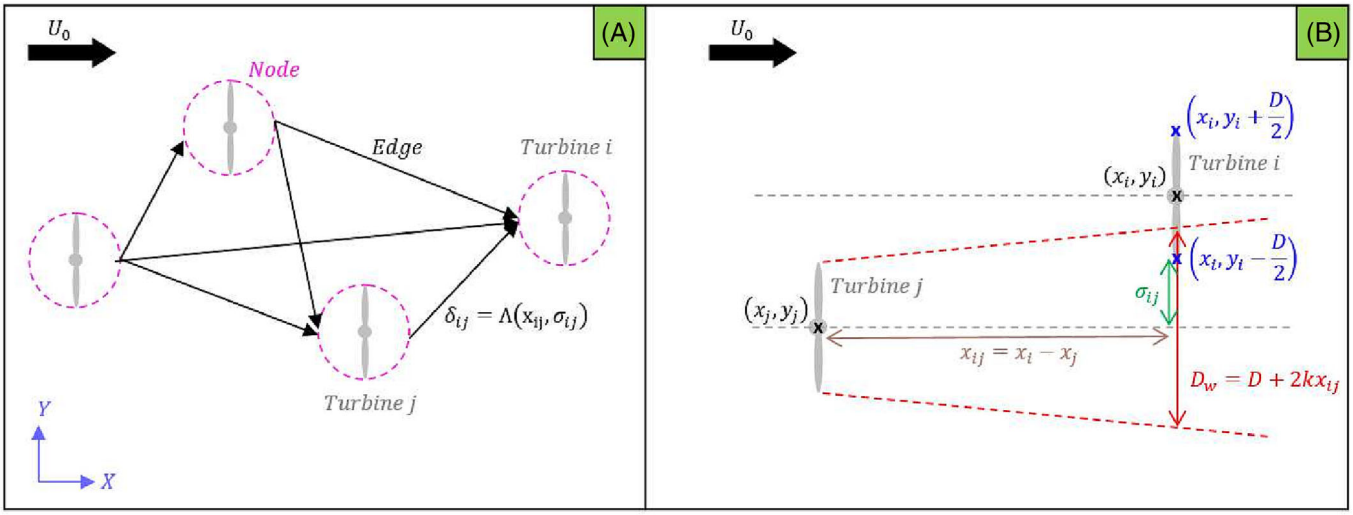

FIGURE 7 A wind farm (WF) presented as a direct network in (A), where each turbine is a node and the edges are weighted δ_{ij}. Panel B shows an example of the wake of turbine *j* affecting turbine *i* and the different parameters.

Algorithm 1 RNF algorithm

Require: The WF set of turbines Ω and a selected turbine *i*

Require: Ω must be descent sorted in the wind direction (downstream to upstream)

1: $\Omega_i \leftarrow \{i\}$ > Initialize the subset Ω_i; Contains only turbine i for now
2: $\Omega \leftarrow \Omega \setminus \Omega_i$ > Omit *i* from the WF set
3: Compute $X(j) = (x_{ij}) \quad \forall j \in \Omega$ > *X* is a vector of x_{ij} elements
4: Compute $\Sigma(j) = (\sigma_{ij}) \quad \forall j \in \Omega$ > Σ is a vector of σ_{ij} elements
5: $\Delta(j) = \delta_{ij} \leftarrow \Lambda(x_{ij}, \sigma_{ij}) \quad \forall j \in \Omega$ > Δ is a vector of δ_{ij} elements
6: **if** $\exists \delta_{ij}$ is True **then** > If there are neighbors *j* of *i*
7: **loop** for each neighbor *j* of *i*
8: $\Omega_j \leftarrow$ **Call** the **RNF Algorithm** > RNF calls itself with Ω and turbine *j*
9: $\Omega_i \leftarrow \Omega_i \cup \Omega_j$ > Add the subset neighbors of *j* in the subset *i*
10: $\Omega \leftarrow \Omega \setminus \Omega_j$ > Omit the subset Ω_j from Ω
11: **end loop**
12: **end if**
13: **Return** Ω_i

To validate the static wake model and assess the four algorithms in terms of accuracy and computation time, a WF case study is needed. Such a case study inspired by the Belgian Mermaid offshore WF[21] is presented in the next section.

5 | THE MERMAID WF STUDY CASE

5.1 | The mermaid WF and its wind data statistics

The layout of the Belgian 235 MW Mermaid offshore WF[21] is depicted in Figure 8. It comprises 28 WTs with a rotor diameter of $D_{Md} = 167$ m and a power capacity of 8.4 MW. Due to the tight area for Belgian offshore WFs, it can be noticed that the distance between turbines is in the range $[3D; 6D]$. In this research, the 5MW-NREL HAWT with a rotor diameter $D = 126$ m is the reference since we are using the FAST.Farm software. To account for this specific WT, the rules of similarity introduced by Garsch et al[38] must be respected. Assuming they hold true, the geometrical scaling factor ν to be used is equal to $\frac{D}{D_{Md}} \approx 0.75$. The scaling of the power is proportional to ν^2, leading to a power capacity of 4.8 MW, which is reasonably close to the 5 MW capacity of the reference WT in the actual study. This difference comes from the violation of at least one of the rules of similarity, such as the blade profile which may not be the same for both WTs, as it is not available for the Mermaid WTs. Nevertheless, in the absence of more information, the considered case study is obtained as a geometrical scaled layout on

10991824, 2023, 8, Downloaded from https://onlinelibrary.wiley.com/doi/10.1002/we.2845 by EVIDENCE AID - BELGIUM, Wiley Online Library on [03/10/2023]. See the Terms and Conditions (https://onlinelibrary.wiley.com/terms-and-conditions) on Wiley Online Library for rules of use; OA articles are governed by the applicable Creative Commons License

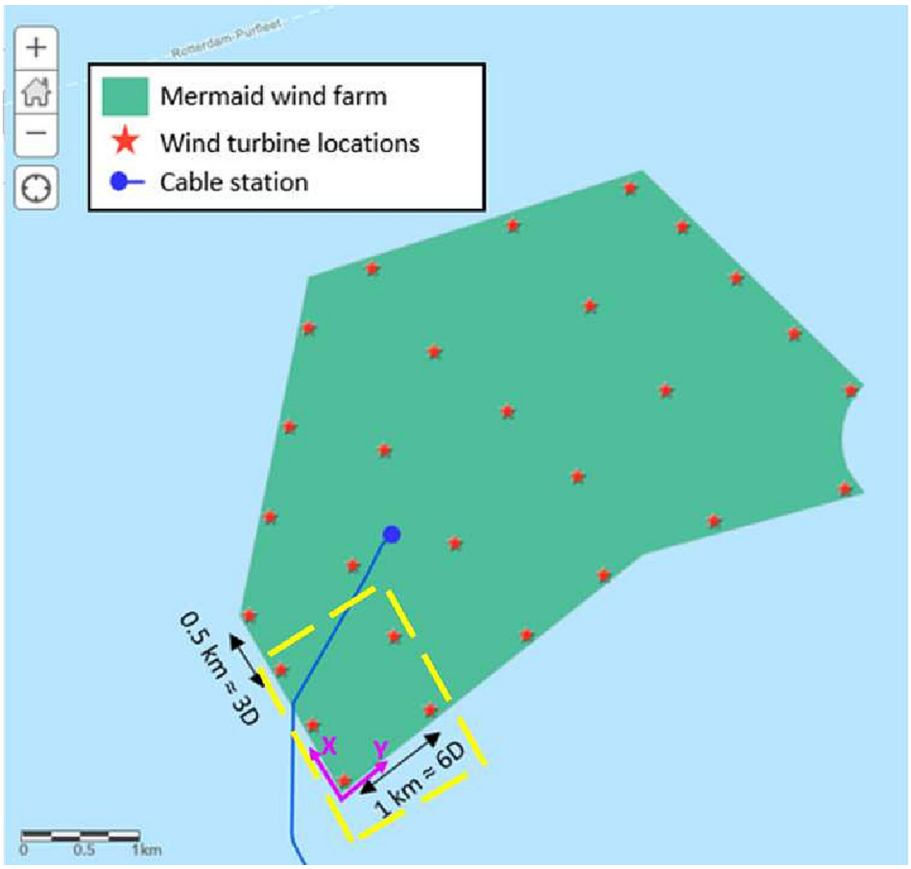

FIGURE 8 Belgian Mermaid offshore wind farm.[21]

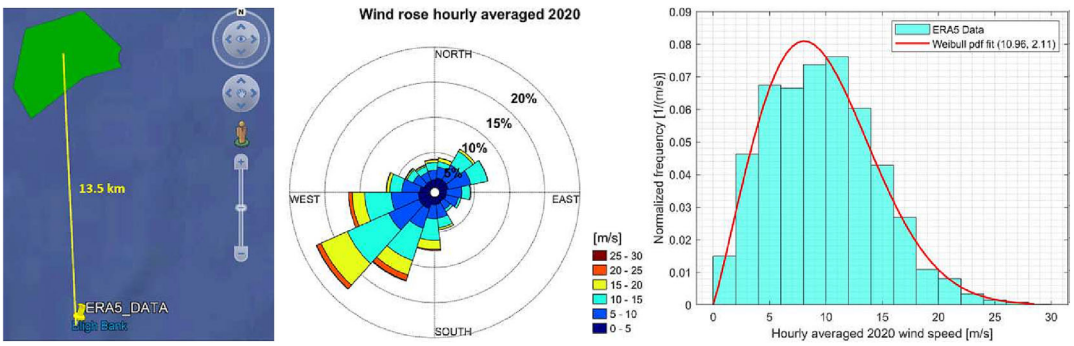

FIGURE 9 ERA5 data location from Mermaid wind farm (WF) site (left); wind rose hourly data 2020 (middle); hourly 2020 wind speed normalized histogram and its fitted Weibull probability density function (right).

which each turbine corresponds to the 5MW-NREL HAWT, leading to a WF capacity of 140 MW. Knowing that the minimum distance between neighboring turbines is higher than 3*D*, we consider that the far wake model presented previously is suitable to represent wake effects between WTs.

Wind data statistics at the site are needed, and the open-source Copernicus Climate Data Store ERA5[39] was used for this purpose. A total of 366 days of atmospheric hourly data of the year 2020 around the WF site, at 90 m height, is supplied by ERA5, and its statistics are given in Figure 9.

These data correspond to a site located around 13.5 km away from the WF as shown in Figure 9. The wind rose shows that the wind comes mainly from South-West, with the largest inner distance between the WTs and smallest overall wake effect. Finally, the normalized wind speed histogram follows a Weibull law with (10.96,2.11) as scaling and shape parameters, respectively.

10991824, 2023, 8, Downloaded from https://onlinelibrary.wiley.com/doi/10.1002/we.2845 by EVIDENCE AID - BELGIUM, Wiley Online Library on [03/10/2023]. See the Terms and Conditions (https://onlinelibrary.wiley.com/terms-and-conditions) on Wiley Online Library for rules of use; OA articles are governed by the applicable Creative Commons License

5.2 | Validation of the wake model

For the validation of the wake model, two cases are considered. The first one is based on steady wind flow data as used for parameter estimation algorithm of Section 3.2.2. In the second test case, the performance of the static wake model for predicting the average output power of the WTs for a turbulent wind flow is investigated.

From now on, the so-called "Greedy" and "Cooperative" approaches will be distinguished. In the "Greedy" approach, all the WTs maximize their individual power and are thus yawed in the wind direction. In the "Cooperative" approach, the WTs are controlled in order to maximize the overall WF power through yaw optimization.

Focusing on the first case, an example of the comparison between the model and FAST.Farm data is given Figure 10 with $X = 6D, Y \in \{-D; 0; D\}$, and $U_0 = 8$ m/s. With $Y = -D$ and looking only at the positive yaw angles of the first turbine $(\gamma_1 > 0^\circ)$, the power of the second turbine is increasing as γ_1 increases. This is due to the wake that slightly affects the second turbine at $\gamma_1 = 0^\circ$ and is directed away thanks to the yawing of the first turbine. Besides, it can be seen that there exists an optimal yaw angle where the sum of the powers of both WTs is higher than the classical configuration with $\gamma_1 = \gamma_2 = 0^\circ$. Looking at the negative yaw angles $(\gamma_1 < 0^\circ)$ in the same case $Y = -D$, the second turbine is more affected by the wake as γ_1 decreases, since the wake is directed more toward it, such that the total power decreases. A similar observation holds in the third case with $Y = D$ by symmetry with respect to the X axis. In the second case $Y = 0$, yawing positively or negatively the upstream WT leads to directing the wake away from the downstream turbine, resulting in a global power increase.

Looking at the power outputs of the WTs, a good match is seen between the model and FAST.Farm focusing on the cases $(Y = 0), (Y = -D, \gamma_1 > 0)$ and $(Y = D, \gamma_1 < 0)$ in Figure 10. Indeed, the separate WT powers given by the model are close to the ones from FAST.Farm, and the total power trend is the same. For the cases where $(Y = -D, \gamma_1 < 0)$ and $(Y = D, \gamma_1 > 0)$, the trend and the total WF power are acceptable as they are close to FAST.Farm, and the WF power decreases with the change of γ_1. However, there is a disagreement in the power trend of Turbine

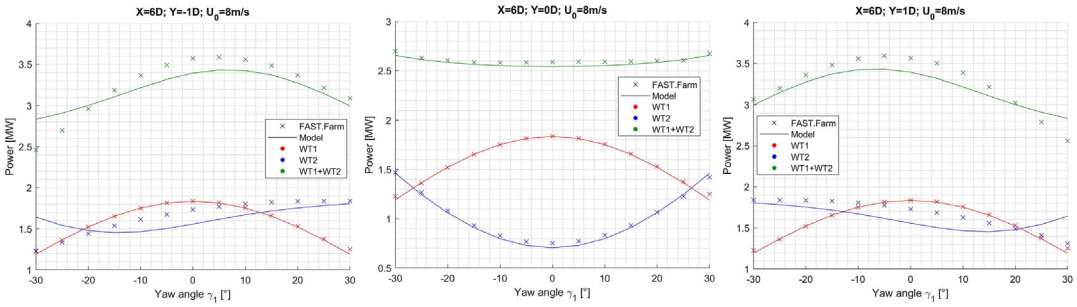

FIGURE 10 Comparison between the model (line) and FAST.Farm (cross) in terms of power outputs. The red color represents the upstream WT1, the blue color represents the waked WT2, and the green color represents the wind farm (WF) power.

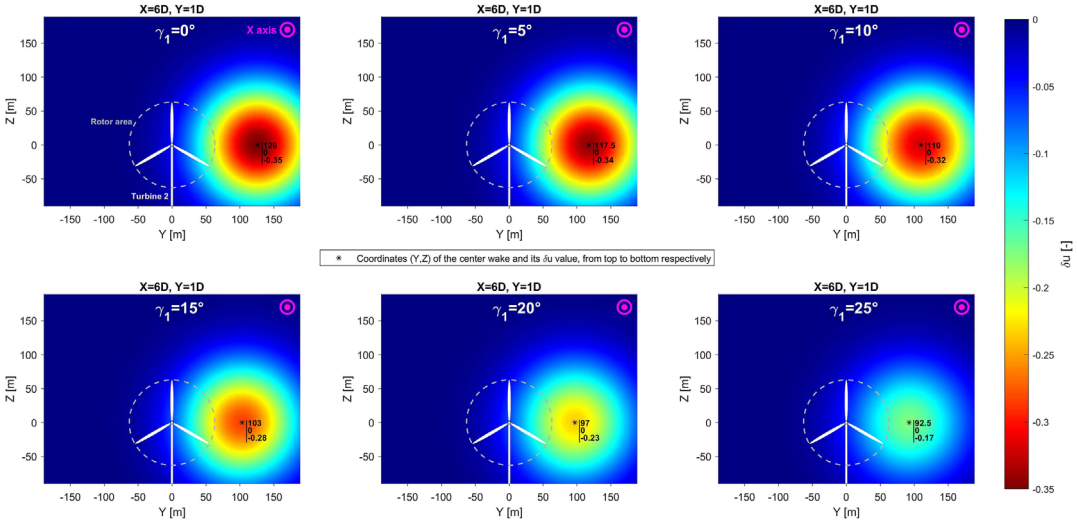

FIGURE 11 Variation of the wake deficit δu in the rotor plane of WT2, when γ_1 increases, for the case $(X = 6D, Y = 1D, \gamma_1 > 0)$. The black star marker indicates the value and the coordinates (Y, Z) of the wake center and its value $-|\delta u|_{Max}$, from top to bottom, respectively.

10991824, 2023, 8, Downloaded from https://onlinelibrary.wiley.com/doi/10.1002/we.2845 by EVIDENCE AID - BELGIUM, Wiley Online Library on [03/10/2023]. See the Terms and Conditions (https://onlinelibrary.wiley.com/terms-and-conditions) on Wiley Online Library for rules of use; OA articles are governed by the applicable Creative Commons License

2. Indeed, it is noticeable that the power of Turbine 2 from the model decreases until $|\hat{\gamma}_1| \sim 12^\circ$, then it starts to increase again. This disagreement comes from the *cosine* in the expression of the wake deficit δu (2), inducing a decrease in the wake deficit amplitude when the yaw angle increases, as can be seen in Figure 11. The plots present how the wake deficit δu changes spatially in Turbine 2 rotor plane, when γ_1 increases, for the case $(X = 6D, Y = D, \gamma_1 > 0)$. The black star marker indicates the coordinates (Y, Z) of the wake center and the value of the wake deficit at that location $-|\delta u|_{Max}$, from top to bottom, respectively. It is clear that the wake center deviates toward the downstream turbine, and the maximum amplitude of $|\delta u|$ decreases, as γ_1 increases. Therefore, even though Turbine 2 is more waked with the increase of γ_1, there is a specific $\hat{\gamma}_1$ where the wake deficit amplitude drops drastically due to the *cosine* in (2), inducing a lower impact of the wake and thus an increase of the output power.

To conclude with, even if there is this slight disagreement, the model represents well the output powers of the WTs in steady wind conditions, with a mean error of 0.4% with respect to the WT nominal power (5 MW) and a standard deviation of 2% at the WT level. Besides, the global power output trend is respected. Finally, the optimal yaw angle for power maximization is found to be the same from both the model and FAST.Farm.

In the second case, aimed at testing the validity of our tuned static model in a turbulent wind case, the following WT configuration is considered. Five WTs within the Mermaid WF are selected, which are within the yellow rectangle sketched in Figure 8. Only five WTs are taken for simplicity and reduction of the computation time in FAST.Farm. Besides, the most waked case (i.e., with wind in the X direction) is chosen for the assessment, having a mean wind speed of 8 m/s, and a TI of 6%, representing offshore wind conditions at the North Sea.[40] In Figure 12, both the inflow wind of the greedy (left) and the cooperative (right) approaches simulated with FAST.Farm are depicted. It can be clearly noticed that the wake is redirected in the cooperative approach, leading to higher wind speeds upstream the downstream WTs.

The results of the simulations in terms of produced power are given in Figure 13. The red and green bars represent the averaged output powers from FAST.Farm for the greedy and the cooperative approaches, respectively. More precisely, the average is computed over a horizon of 10 min for data recorded after letting the simulation run for 20 min, which ensures steady state is reached. The blue and purple bars give the output powers from the static model considered in our study for the yaw optimization method. The trends in the power output between the different turbines and depending on the greedy or cooperative approach are maintained for the simplified wake model. Looking at the WF power, which is the most important variable to predict for yaw optimization, it can be observed that the simplified wake model underestimates the WF power by 5.6% in the greedy approach and by 1.5% for the cooperative approach. This underestimation puts us on the safe side for power reserve estimation with the simplified wake model. Notice that most errors are within the waked WTs. This results from the dynamics of the inflow wind (e.g., turbulence and meandering) and the errors from the simplified static model.

5.3 | Comparison of the yaw optimization algorithms

In order to compare the four algorithms at hand, the power gain is computed through the difference between the Greedy and the Cooperative approaches in all the wind directions θ_w, with $U_0 = 10$ m/s. Note that the latter represents the annual mean wind speed of the dataset Figure 9. The resulting power gain rose is presented in the left subplot of Figure 14, starting at 0° from South-East (X-wise in Figure 8) with an increment of 1°, and anticlockwise until 360°. The right subplot of Figure 14 gives the computation time of each algorithm depending on the wind direction, in a natural logarithmic scale. Around 0°, the distance between the WTs is minimal ($\sim 3D$) leading to a maximum wake effect, while around 270°

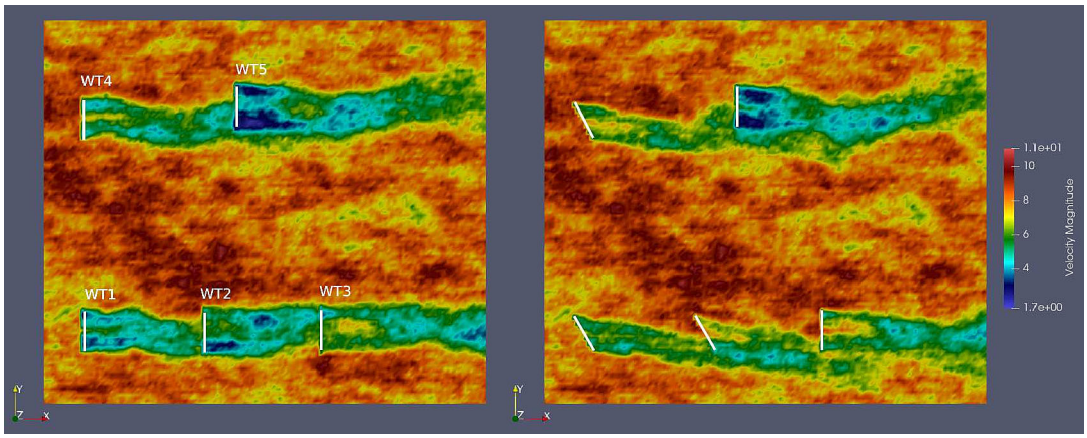

FIGURE 12 Top view of the greedy (left) and cooperative (right) approaches in a wind farm (WF) of five wind turbines (WTs), simulated in FAST.Farm, under a wind flow of 8 m/s mean wind speed, and 6% TI, at 30 min simulation time.

10991824, 2023, 8, Downloaded from https://onlinelibrary.wiley.com/doi/10.1002/we.2845 by EVIDENCE AID - BELGIUM, Wiley Online Library on [03/10/2023]. See the Terms and Conditions (https://onlinelibrary.wiley.com/terms-and-conditions) on Wiley Online Library for rules of use; OA articles are governed by the applicable Creative Commons License

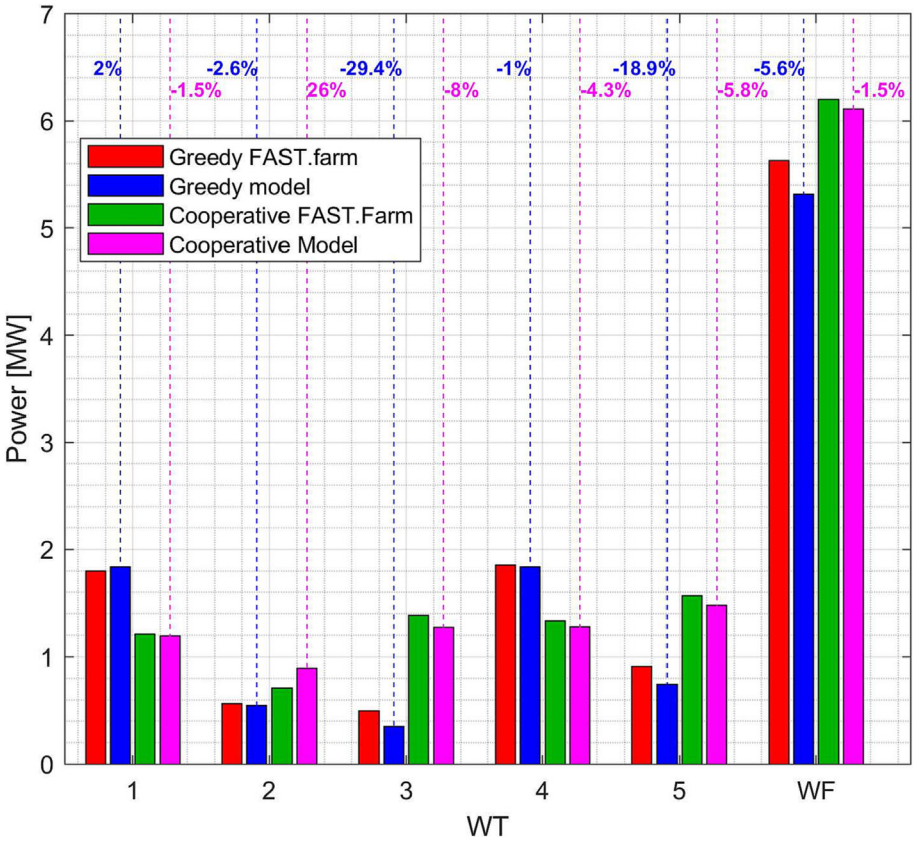

FIGURE 13 Power outputs for the greedy and cooperative approaches, from FAST.Farm averaged in 10 min and from the static wake model.

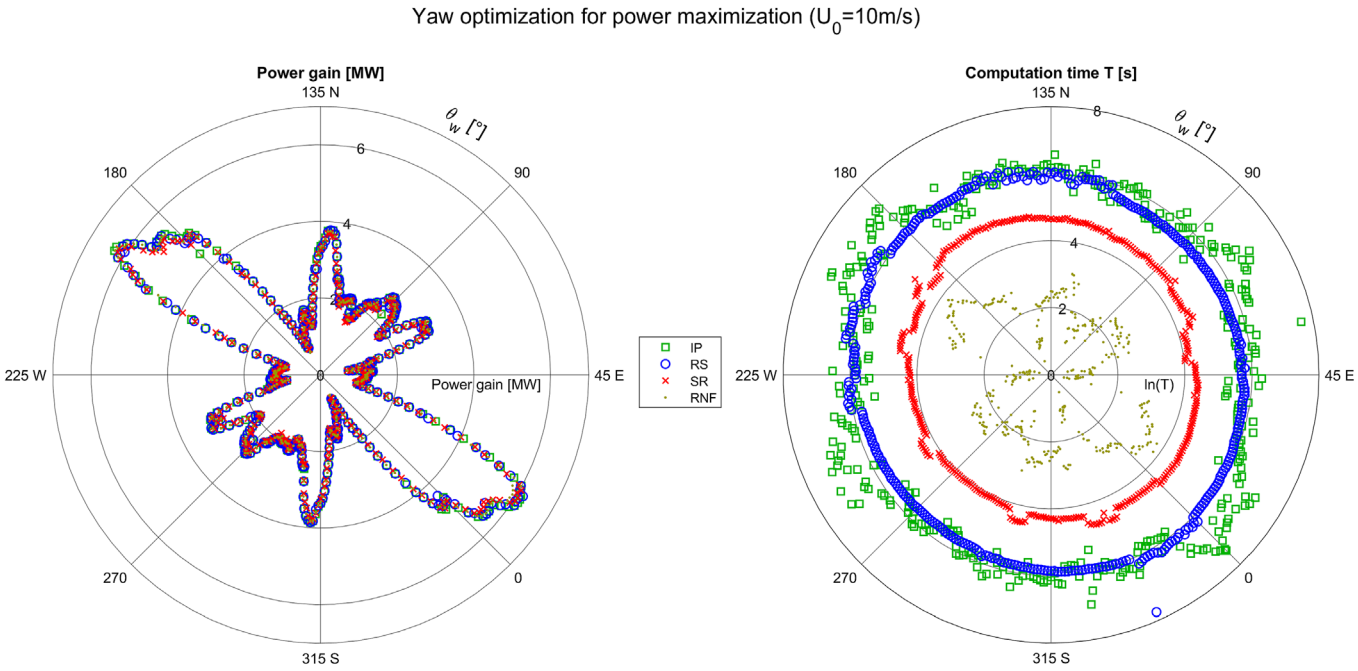

FIGURE 14 Power gain rose computed for the Mermaid wind farm (WF) by the three algorithms (left) and their computation time (right).

10991824, 2023, 8, Downloaded from https://onlinelibrary.wiley.com/doi/10.1002/we.2845 by EVIDENCE AID - BELGIUM, Wiley Online Library on [03/10/2023]. See the Terms and Conditions (https://onlinelibrary.wiley.com/terms-and-conditions) on Wiley Online Library for rules of use; OA articles are governed by the applicable Creative Commons License

(*Y*-wise in Figure 8), the inner distance is maximal ($\sim 6D$) leading to the least wake effect (most frequent wind direction yearly, Figure 9). These last two cases will be called "most waked case" and "most dominant case", respectively.

Focusing on the left subplot of Figure 14, it is clear that the four algorithms give almost the same power gain, for all the wind directions. Note that the highest power gain is obtained within the most waked case, where the wake interaction is mostly present. Regarding the computation time, it has been evaluated on a laptop having the specifications presented in Table 4. Significant differences can be observed. The slowest algorithm in most of the wind directions is the IP; its computation time varies between 5 and 30 min. The computation time of the RS algorithm varies slightly around 5 min, and this is in accordance with the fixed number of iterations. The SR algorithm outperforms the two other centralized ones with a computation time around 1 min. The RNF algorithm invariably computes the power gain in less than 1 min, which outperforms the three centralized algorithms. The mean computation time in all the wind directions is summarized in Table 5.

The power gain percentage error (*PG_Err*) of RS, SR, and RNF algorithms relative to the IP method can now be determined. IP is taken as a reference since it is centralized and gives the highest WF power for almost all wind directions. Figure 15 depicts *PG_Err* and shows that it can go

TABLE 4 Some characteristics of the laptop.

Hardware	Specifications
Processor	6-core 2.59 GHz
RAM	64 Go

TABLE 5 Mean computation time in all the wind directions of the optimization algorithms.

Algorithm	IP	RS	SR	RNF
Mean computation time (s)	514.34	362.88	85.96	11.56

Abbreviations: IP, interior-point; RNF, recursive neighbor function; RS, random search; SR, serial-refine.

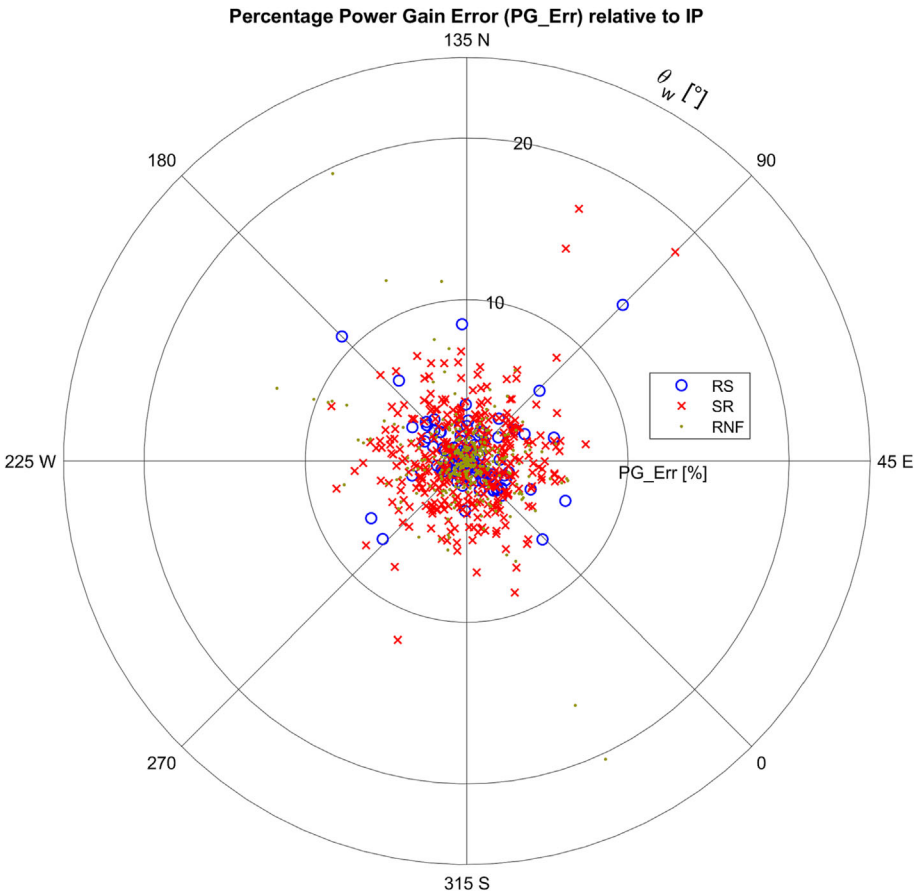

FIGURE 15 Percentage error relative to the IP centralized optimization algorithm, for the Mermaid wind farm (WF).

10991824, 2023, 8, Downloaded from https://onlinelibrary.wiley.com/doi/10.1002/we.2845 by EVIDENCE AID - BELGIUM, Wiley Online Library on [03/10/2023]. See the Terms and Conditions (https://onlinelibrary.wiley.com/terms-and-conditions) on Wiley Online Library for rules of use; OA articles are governed by the applicable Creative Commons License

from 0% up to 13.7%, 18.3%, and 20.4% for RS, SR and RNF algorithms respectively. The average *PG_Err* in all the wind directions is 0.68%, 3.48%, and 2.2% respectively, leading to note that SR is, on average, the least accurate among these three algorithms, due to the discrete yaw angles set through the variable N_{yaws}. If the latter is increased for more accuracy, the algorithm will be more time-consuming. Focusing on the RNF algorithm, a significant variation in the computation time and the errors can be observed with the wind direction. This can be explained by the variable number of WTs within each subset. Indeed, in some directions, the subsets are large, leading to a higher computation time. Moreover, due to the wake recovery assumption of 10D (see point 4a in the computation of δ_{ij}), errors in the power gain are larger in some directions than others. Finally, even though the RS centralized algorithm is more accurate than the distributed one, the errors of the RNF algorithm are still acceptable (less than 0.1 MW) as presented in Table 6. Consequently, the trade-off between the accuracy of the power gain and computation time leads to choose the distributed optimization algorithm.

While Annoni et al[36] work accounts for wake interaction between subsets having at least one turbine in common, the RNF algorithm considers disjoint subsets. Besides, the edge criterion proposed in their work is based on the overlap area between the wake effect generated by an upstream turbine and the rotor disk of the waked turbine, which is different from the RNF edge criterion. Even though Annoni et al. study case is different from ours, the order of magnitude of *PG_Err* is similar. Indeed, Annoni et al[36] simulated two wind directions in their study case resulting in a *PG_Err* of 0.56% and 33%, which are in the same range as the RNF algorithm Figure 15. Consequently, despite not considering subsets interactions, the RNF algorithm performs well in terms of accuracy and computation time, and will be our main tool to assess participation in FRR, both in terms of power bid and time response requirements defined by Elia.

.

5.4 | Power gain assessment for yaw optimization-based FRR

As indicated in Section (3), we restrict our study to WT operation in zone 2, which corresponds to $U_0 \in [7.85; 10.24]$ m/s. In order to compute the power gain resulting from yaw optimization in this wind speed range, notice that the overall wake deficit on WT_i, $\delta\widehat{u_i}$ in (8), does not depend of

TABLE 6 Absolute mean error and RMSE of the RS and RNF algorithms, over all wind directions.

Algorithm	|Mean error value| (MW)	RMSE value (MW)
RS	0.016	0.058
SR	0.074	0.070
RNF	0.048	0.059

Abbreviations: RNF, recursive neighbor function; RS, random search; SR, serial-refine.

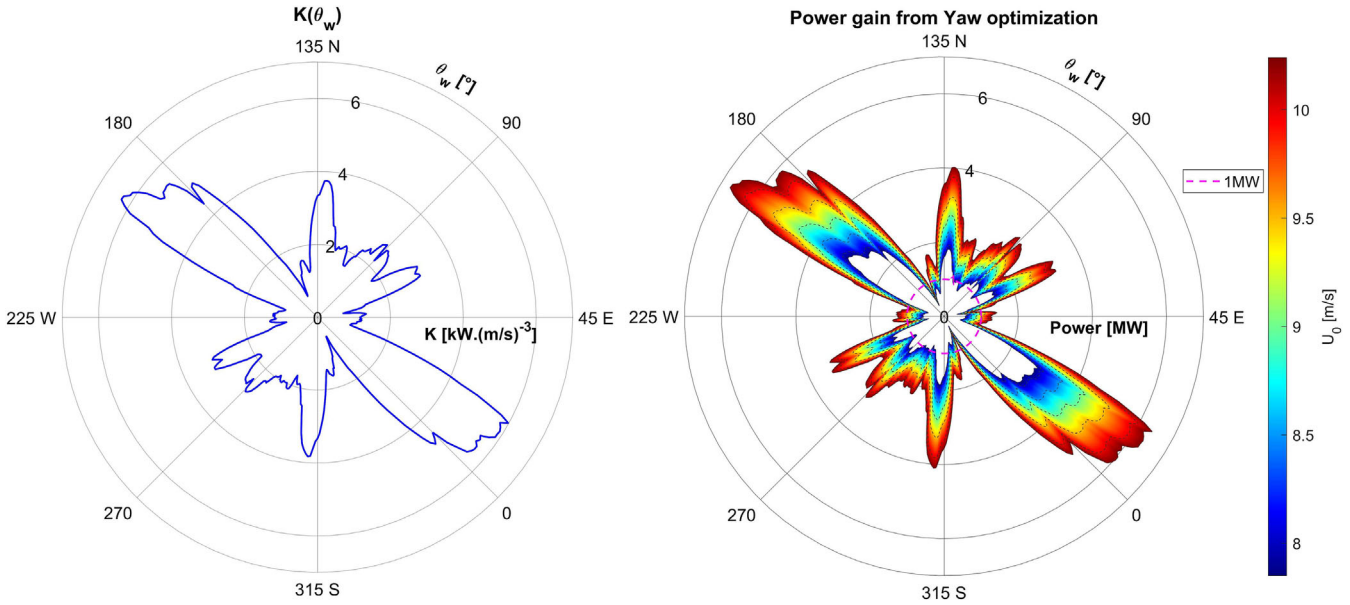

FIGURE 16 The left subplot shows the dependence of *K* on the wind direction. The right subplot gives the resulting power gain rose for the considered wind speed range.

10991824, 2023, 8, Downloaded from https://onlinelibrary.wiley.com/doi/10.1002/we.2845 by EVIDENCE AID - BELGIUM, Wiley Online Library on [03/10/2023]. See the Terms and Conditions (https://onlinelibrary.wiley.com/terms-and-conditions) on Wiley Online Library for rules of use; OA articles are governed by the applicable Creative Commons License

the free wind speed. Therefore, for a specific wind direction θ_w and free wind speed U_0, the maximum power gain through yaw optimization of the WF $\Delta P_{WF}(\theta_w, U_0)$ is computed by the following:

$$\begin{aligned}\Delta P_{WF}(\theta_w, U_0) &= P^*_{WF}(\theta_w, U_0) - P^0_{WF}(\theta_w, U_0) \\ &= \frac{1}{2}\eta\rho\pi R^2 C_{pMax}\left[\sum_{i=1}^{N}\left(1-\delta\widehat{u}_i{}^*(\theta_w)\right)^3 cos^3\left(\gamma_j^*(\theta_w)\right) - \sum_{i=1}^{N}\left(1-\delta\widehat{u}_i{}^0(\theta_w)\right)^3\right]U_0^3 \\ &= K(\theta_w)U_0^3,\end{aligned} \tag{17}$$

where the superscripts (*) and (^{0}) stand for values obtained from the cooperative and the greedy approaches, respectively, and with $K(\theta_w)$ depending only on θ_w:

$$K(\theta_w) = \frac{1}{2}\eta\rho\pi R^2 C_{pMax}\sum_{i=1}^{N}\left[\left(1-\delta\widehat{u}_i{}^*(\theta_w)\right)^3 cos^3\left(\gamma_j^*(\theta_w)\right) - \left(1-\delta\widehat{u}_i{}^0(\theta_w)\right)^3\right]. \tag{18}$$

The factor $K(\theta_w)$ can be found by dividing the power gain through yaw optimization obtained previously, in the case of $U_0 = 10$ m/s, by U_0^3. The value of $K(\theta_w)$ and the power gain through yaw optimization, within the considered wind speed range, are presented in Figure 16. Looking at the most waked case, the maximum power gain is higher than 2 MW for all the wind speeds. Focusing on the dominant case, most of the wind directions enable a power reserve higher than 1 MW for all the considered wind speed range, but it can be noticed that there are some specific wind directions where for U_0 lower than 8.5 m/s, the maximum power gain is not high enough to participate in the utility grid. Finally, around the most frequent wind speed, namely, 10 m/s, the power reserve is high enough to participate in the utility grid for almost all the wind directions.

Given our observations regarding the impact of turbulence on the output power, we can expect similar or even slightly larger power gains for a turbulence intensity of 6%. Furthermore, applying the rules of similarity presented in Section 5.1, we can refer to a WF having WTs with the same rotor diameter as the Mermaid ones $D_{Md} = 167$ m. The latter rules will induce the power gain Figure 16 to increase by a power scaling factor of $\iota = \left(\frac{1}{\nu}\right)^2 \approx 1.76$. However, the WF capacity induced by this factor is 245.9 MW, which is 4.5% higher than the actual Mermaid WF. The power scaling factor resulting from the WF capacities is $\iota = \frac{235.2}{140} \approx 1.68$. Consequently, the power gain of the Mermaid WF will be at least 1.68 higher than the one found in Figure 16, enabling more power reserve margin to participate in FRR.

5.5 | Time scale assessment for yaw optimization-based FRR

Knowing that the participation of WFs in FRR through yaw optimization methods seems feasible in terms of power reserve, the question of time response is addressed in this section. The time required for reaching a steady power output once the optimization algorithm is triggered can be estimated by adding up the following contributions:

1. RNF algorithm computing time
2. Yaw actuation response time
3. Wake effect stabilization

These three points are successively considered. First, as shown in Figure 14, the RNF algorithm can be executed in less than 60 s ($ln(T) \leq 4, T$ in seconds). Moreover, actual yaw actuators of the three bladed HAWT have a maximum yaw rate around 0.5°/s.[41] The 5MW-NREL WT has a maximum yaw rate of 0.3°/s. Knowing that yaw angle changes up to around 30° for WF power maximization through yaw optimization,[18–20] the yaw actuator response time can be up to 100 s, assuming an initial position corresponding to the greedy approach. Finally, to determine the longest wake traveling time, the maximum distance between the most upstream and most downstream waked WTs within a subset must be found. To do so, the RNF algorithm is used to find the highest wake traveling distance considering all wind directions and all subsets. This worst case is illustrated in Figure 17 where WTs 15 and 12 in subset number 6 are 3.22 km apart.

To estimate the wake traveling time within the latter subset, the four turbines are simulated in FAST.Farm, making them completely aligned to get the full wake case and thus the highest wake deficits. The downstream turbines 14, 13, and 12 are distant from the most upstream one, 15, by 8.12D, 16.94D, and 25.54D, respectively. These turbines will be noted as WT1, WT2, WT3, and WT4 sorted from the most upstream one. Two simulations are performed: The first one considers only an incoming steady wind of 8 m/s, which is a low wind speed in the second operation region of the 5MW-NREL WT. In the second simulation, a TI of 6% is added to the incoming wind with mean wind speed equal to 8 m/s. The effective wind speeds are depicted in Figure 18 for the WTs, in steady (top left) and turbulent (top right) cases. The effective wind speed is defined as the averaged wind velocity within the rotor disk of a WT. In the top right plot of Figure 18, the turbulent data are smoothed thanks to the moving mean method, with a window of 10 min.

10991824, 2023, 8, Downloaded from https://onlinelibrary.wiley.com/doi/10.1002/we.2845 by EVIDENCE AID - BELGIUM, Wiley Online Library on [03/10/2023]. See the Terms and Conditions (https://onlinelibrary.wiley.com/terms-and-conditions) on Wiley Online Library for rules of use; OA articles are governed by the applicable Creative Commons License

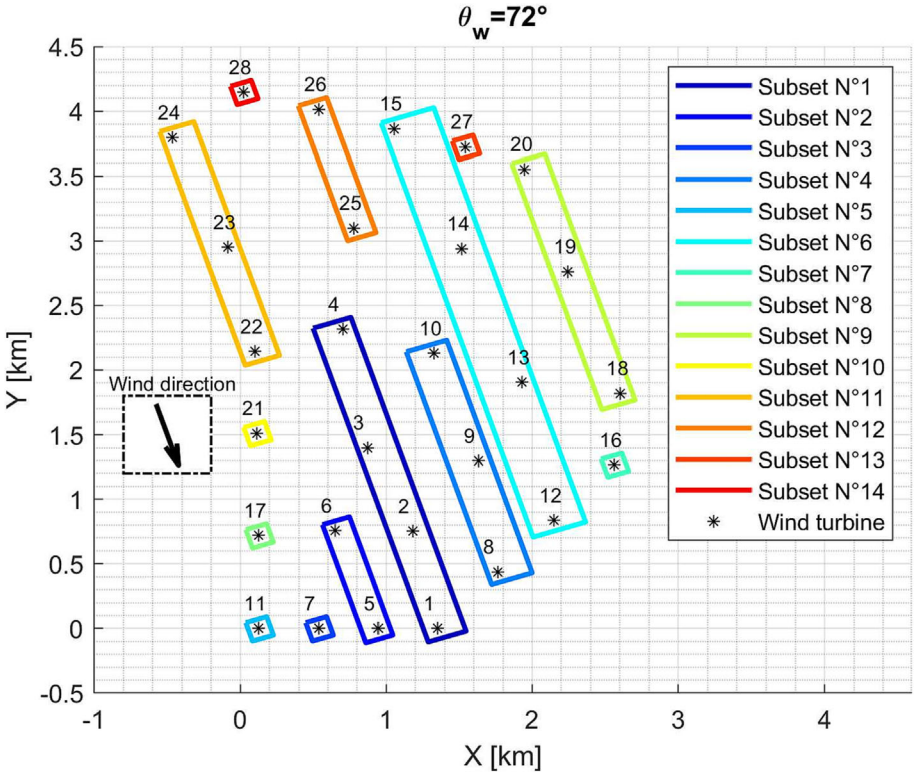

FIGURE 17 The wind direction 72° where subset 6 involves the highest wake traveling distance (between wind turbines [WTs] 15 and 12).

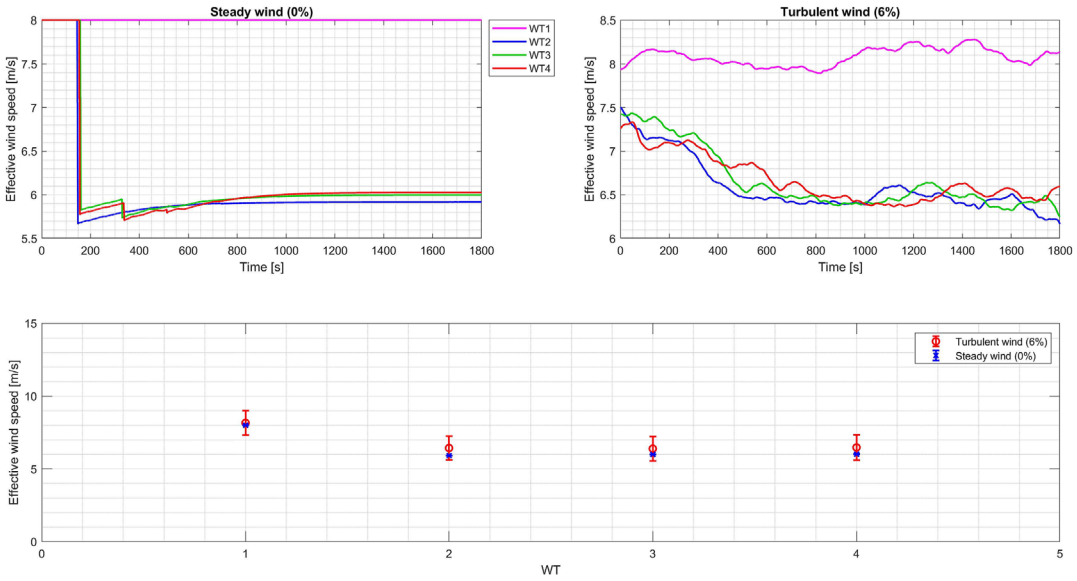

FIGURE 18 Effective wind speeds variations in time at the rotor disks of the wind turbines (WTs). Top left: steady wind case; top right: smoothed turbulent case using a moving mean method having a window of 10 min; bottom: the means and standard deviations of the raw data in both cases.

Focusing first on the steady wind condition, the simulation starts (t =0 s) with the 8 m/s wind speed within the whole WF, with no wake propagation. As the simulation goes on ($t >$ 0s), the generated wakes of the WTs propagate. Looking at the most downstream WT (WT4), it is affected by the wakes from WT3, WT2, then WT1 consecutively. The latter phenomenon can be noticed in the upper left plot of Figure 18, from the successive drops of the effective wind speed of WT4 at 156 s, 336 s, and 512 s. Consequently, the traveling time of the wake generated by WT1 to arrive to WT4 is 512 s, representing a mean wake traveling velocity of 6.26 m/s. This velocity is close to the average effective wind speed

10991824, 2023, 8, Downloaded from https://onlinelibrary.wiley.com/doi/10.1002/we.2845 by EVIDENCE AID - BELGIUM, Wiley Online Library on [03/10/2023]. See the Terms and Conditions (https://onlinelibrary.wiley.com/terms-and-conditions) on Wiley Online Library for rules of use; OA articles are governed by the applicable Creative Commons License

upstream WT4 in the turbulent case, which is equal to 6.48 m/s. This value is obtained by computing the average over the last 10 min of the raw turbulent data and is depicted in the lower plot of Figure 18. The latter plot provides the means and standard deviations of the raw effective wind speed data upstream each WT. Notice that the mean effective wind speed is almost the same for all the downstream turbines, around 6.4 m/s in the turbulent wind case. This can be explained by the fading of the wake deficit at the very far wake. Indeed, the effective wake deficit $\delta\hat{u}_i$ at a downstream turbine i, introduced previously in Equation (8), depends on the wake deficits $\delta\bar{u}_{ij}(x_{ij})$ generated by the upstream turbines j. For WT2, the effective wake deficit is $\delta\hat{u}_2 = \delta\bar{u}_{12}(8.12D)$, leading to a mean effective wind speed of around 6 m/s. For WT3, the effective wake deficit is $\delta\hat{u}_3 = \sqrt{\delta\bar{u}_{13}^2(16.94D) + \bar{u}_{23}^2(8.82D)}$. Because $\delta\bar{u}_{ij}(x_{ij})$ is roughly proportional to $\frac{1}{x_{ij}^2}$ in the far wake, $\delta\bar{u}_{13}^2(16.94D)$ becomes negligible compared with $\bar{u}_{23}^2(8.82D)$. The latter leads to a wake deficit $\delta\hat{u}_3$ close to $\delta\hat{u}_2$, since the inner distance between WT1 and WT2 is close to the one between WT2 and WT3. Consequently, $\delta\hat{u}_3$ is around 6 m/s as well. The same reasoning goes for the mean effective wind speed for WT4, dominated by the wake deficit of WT3. To sum up, it is estimated that for the mean incoming wind speed of 8 m/s, which is a low wind in the second region of operation of the 5MW-NREL WT, and having a TI of 6%, the mean traveling speed of the wake effect generated by these WTs within this specific assessed case is around 6 m/s. Therefore, the traveling time of the wake effect from WT1 to WT4, which are 25.54D apart and fully waked, is around 537 s. Nevertheless, it can be observed in the turbulent case that the steady state is not reached until around 700 s. At that time and in steady wind conditions, the effective wind speed upstream WT4 is 2% lower than the one reached at the steady state as seen in the upper left plot of Figure 18. Consequently, knowing that this assessed case represents the worst-case scenario of having the 4 turbines aligned, which is not exactly the case for subset 6, the waked steady state is estimated to be reached after 700 s.

Coming back to the actual Mermaid WF, the WTs will be more spaced by $\frac{1}{\nu}$, bringing out two complementary statements. On the one hand, the wake traveling distance is higher, which increases the traveling time of the wake. On the other hand, the influence of turbulence will be more present for the recovery of the wake, which may induce a higher wake traveling speed.

For the scaled WF case study, the sum of all these delays representing the worst-case scenarios for the computation time, yaw actuation, and wake traveling is around 14.3 min. Hence, it is within the 15.5 min FRR preparation time response imposed by Elia. Therefore, it can be concluded that for this specific case study, participation of WFs through yaw optimization in the utility grid is feasible in terms of time response for the secondary regulation, FRR.

5.6 | Transient effect in the WF power following yaw optimization

In the previous sections, it has been shown that the yaw optimization-based method could be used as support for FRR, as it fulfils the time delay and the power reserve requirements from Elia. However, the dynamics of the WF during the transient from the greedy approach to the cooperative one have been neglected. The latter are assessed in the present section.

To evaluate the impact of the system dynamics, the same subset of five WTs introduced in Section 5.2 is considered. The wind blows from the South-East direction, for which the wake effect is the most important as the WTs are closer to each other. In this scenario, the shift from the greedy approach to the cooperative one requires that two WTs undergo a change of yaw of 30°, corresponding to the largest considered yaw misalignment.

Simulations are performed in two situations using FAST.Farm. In the first situation, a steady free wind speed of 8 m/s is considered. All WTs operate in the greedy configuration up to time $t = 1440$ s. At that time, a FRR activation signal is sent to the WF operator. Considering the largest computation time of the RNF algorithm, namely, 60 s, the WTs start yawing to their respective optimal yaw angle at $t = 1500$ s, in order to maximize the WF power. The resulting power transient for the total power produced by the five WTs as provided by FAST.Farm is plotted in the upper part of Figure 19 (black line). In the second situation, the same scenario is considered, except that the wind is characterized by a mean free wind speed of 8 m/s to which a 6% TI is superimposed. To exhibit the impact of wind turbulence, 20 different wind realizations are performed. The corresponding produced power computed using FAST.Farm is plotted in the bottom part of Figure 19; the black line corresponds to the mean of the 20 power trajectories and the red region to the 95% confidence region. Notice that the power data provided for the turbulent wind is averaged over 10 min to correspond to synthetic SCADA data.

Focusing on the steady wind situation in Figure 19, a power dip is observed. This occurs when the WTs start yawing to their respective optimal yaw angle and before the cooperative steady state is reached. This transient effect can be explained as follows. When the turbines start yawing, their output power decreases because of the yaw error, while the deviated wake has not propagated enough to induce a power gain from the downstream turbines. A similar observation holds with the turbulent wind, although the turbulence induces a higher produced power and reduces the dip depth on average (see lower plot in Figure 19).

To evaluate whether this dip hampers participation to FRR is not a trivial task, as it depends on the reference power trajectory notably. Here this reference trajectory (gray line in Figure 19) has been determined as follows. From the average free wind speed of 8 m/s, the global produced power of the five WTs has been determined in the greedy and the cooperative cases, by resorting to the wake model of Section 3. To link these two operating points, a ramp-up phase has been introduced in accordance with Elia specifications. Next, the lower confidence bound on this forecasted power has been accounted for (see orange line sketched in Figure 2). This has been translated somewhat arbitrarily by considering a power

10991824, 2023, 8, Downloaded from https://onlinelibrary.wiley.com/doi/10.1002/we.2845 by EVIDENCE AID - BELGIUM, Wiley Online Library on [03/10/2023]. See the Terms and Conditions (https://onlinelibrary.wiley.com/terms-and-conditions) on Wiley Online Library for rules of use; OA articles are governed by the applicable Creative Commons License

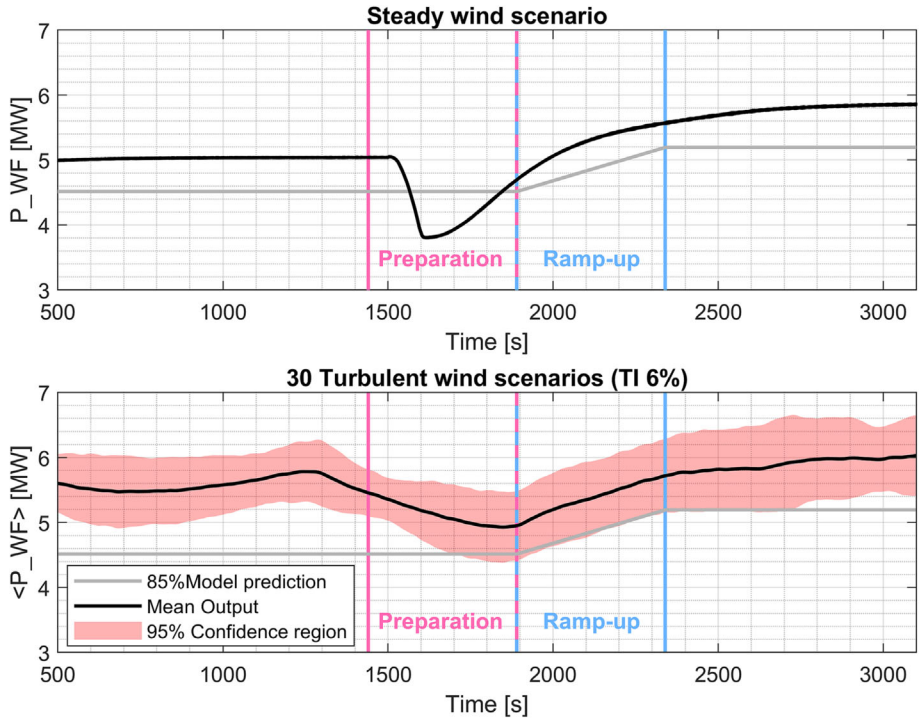

FIGURE 19 Simulations of the transient from the greedy approach to the cooperative one, in steady and turbulent wind scenarios.

reference equal to 85% of the power determined from the wake model. Under these circumstances, it is seen that the average produced power computed by FAST.Farm lies above the power reference in the considered case study. This is explained by the combination of three phenomena: the turbulence effect, the fact that the considered wake model underestimates the maximum available WF power, and the introduction of a margin associated to the confidence bound. Notice however that, in some cases, the required power is not reached during a certain time period, as exhibited by the confidence region. The actual produced power could track the reference power if a proper power controller was implemented, by manipulating the pitch and the generator torque, when the available power is larger than the reference. If the latter condition is not fulfilled, the WF operator should pay for penalties as long as the output power is lower than the reference. Nevertheless, the WF operator can always adjust the power reference to account for the power dip and the accuracy of the wake model used for power prediction. Hence, the WF operator may still be able to participate in FRR despite the power loss during the transient between the greedy and the cooperative approaches.

A similar result can be obtained when looking at the set of four WTs considered for time scale assessment in Section 5.5, with the wind direction indicated in Figure 17. However, in that case, the power gain between the greedy and the cooperative operating mode is marginal. This is probably due to the long distance between the successive WTs.

5.7 | Fatigue load analysis

As previously discussed, wake redirection method through yaw control might be used to support FRR. Nevertheless, the load impact of such method on the WT components must be assessed because increased fatigue loads could induce higher maintenance costs and a shorter WT lifetime. The issue is addressed in this section. To do so, a short-term damage equivalent load (DEL) of 10 min was computed using Mlife software developed by NREL,[42] based on the rainflow counting method applied to the FAST.Farm simulation results. The considered loads are as follows:

- Yaw bearing roll (YawBrMxp) and pitch (YawBrMyp) moments.
- Blade root edgewise (RootMxb1) and flapwise (RootMyb1) moments.
- Tower base roll (TwrBsMxt) and pitch (TwrBsMyt) moments.

The study case chosen here is the same as the one considered for the validation of the wake model in Section 5.2, having the five WTs from the scaled Mermaid WF, with an inflow wind of 8 m/s as mean wind speed and a TI of 6%. The short-term DEL are depicted in Figure 20, comparing the greedy and the cooperative approaches. Notice that there is a load increase in most of the WT components when optimizing the yaw angles for power maximization, especially for the yaw roll moment and the bearing tower base roll moment of the yawed WTs. Indeed, the short-

10991824, 2023, 8, Downloaded from https://onlinelibrary.wiley.com/doi/10.1002/we.2845 by EVIDENCE AID - BELGIUM, Wiley Online Library on [03/10/2023]. See the Terms and Conditions (https://onlinelibrary.wiley.com/terms-and-conditions) on Wiley Online Library for rules of use; OA articles are governed by the applicable Creative Commons License

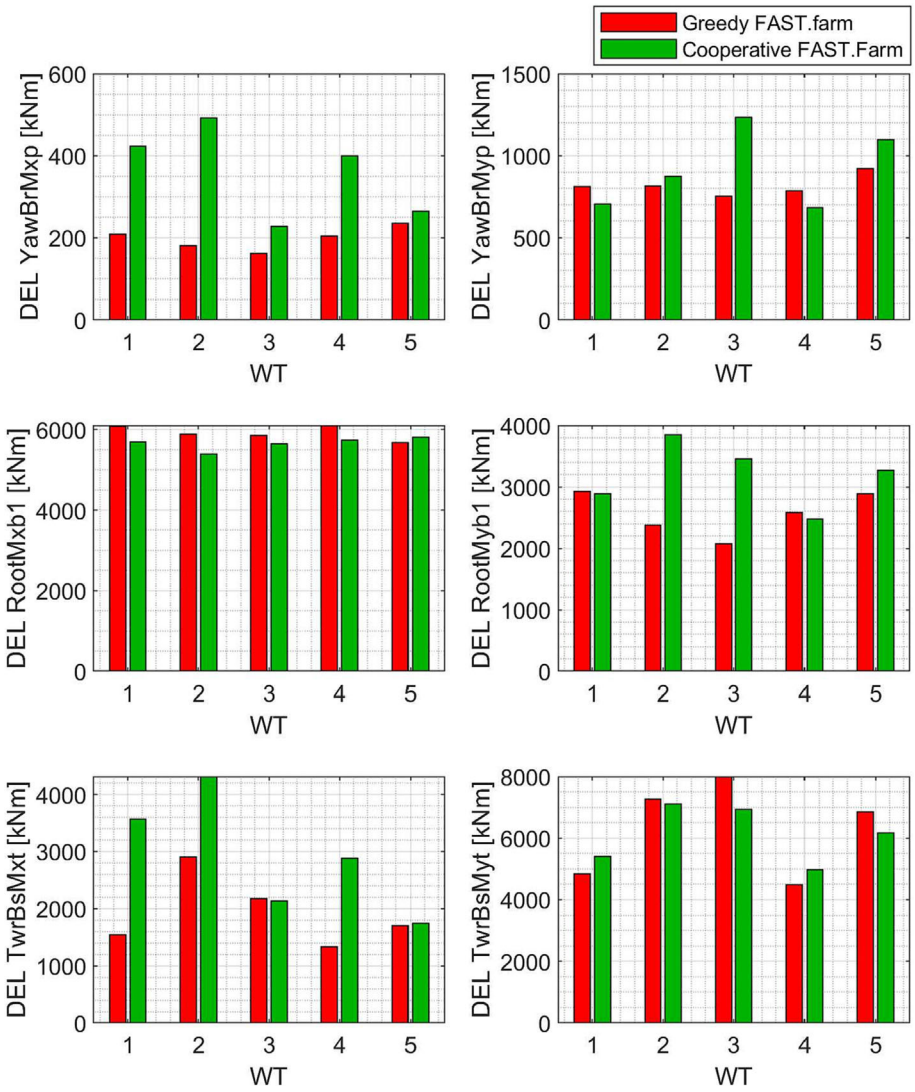

FIGURE 20 Short-term damage equivalent load (DEL) of 10 min of the five considered wind turbines (WTs)

term DEL associated to these moments are multiplied by a factor up to 2.7 and 2.3, respectively. This may be due to the wind misalignment, leading to a higher effective surface on the WT with the contribution of the yawed nacelle and thus higher load moments. From this analysis, we conclude that the yaw optimization for power maximization can be seen as a new power reserve for FRR, but it leads to shortening the lifetime of the WT, by increasing the loads on the WT components that are affected by the yawed operation. However, from frequency data recorded for the Belgian power grid, it appears that the frequency seldom drops below 49.8 Hz. The phenomenon is observed twice over 6 months in the available data set.[43] Therefore, this yaw optimization-based method for FRR should not often be used yearly, so the damages on the WT components may be kept minimal.

6 | CONCLUSIONS

With the goal to participate in the utility grid, WF operators must respect the TSOs requirements in terms of time delay and power bid. This work shows feasibility to achieve the secondary frequency regulation (FRR) by exploiting yaw actuation for decreasing wake effect. To do so, a reliable wake model is built and tuned thanks to the FAST.Farm software. The latter model is used to propose a new distributed yaw optimization algorithm that is faster than the classical centralized yaw optimization methods, while being slightly less accurate. Focusing on a scaled version of the Belgian Mermaid offshore WF as case study, it is shown that the wake steering method is able to respect Elia specifications. Indeed, in terms of time delay, even though the yaw control is very slow in comparison with the pitch and torque control, it is fast enough to achieve the time requirements imposed by Elia for FRR (less than 15 min). In terms of power reserve, the power gain via yaw optimization is higher than the

10991824, 2023, 8, Downloaded from https://onlinelibrary.wiley.com/doi/10.1002/we.2845 by EVIDENCE AID - BELGIUM, Wiley Online Library on [03/10/2023]. See the Terms and Conditions (https://onlinelibrary.wiley.com/terms-and-conditions) on Wiley Online Library for rules of use; OA articles are governed by the applicable Creative Commons License

minimum power bid imposed by Elia (1MW) for all the wind directions at wind speeds close to the most yearly frequent free wind speed. A preliminary study of the effect of the yawing transient indicates that a suitable setting of the FRR power reference is needed in order to account for the induced power dip. Furthermore, higher power gain can be expected for the actual Mermaid WF given the scaling factor. However, the issue of time delay for the actual Mermaid WF should be further studied. These results are promising for WFs operators to enable them to compete with the traditional power plant operators, using not only the pitch and torque controls but also the support of the yaw control. Nevertheless, it should be highlighted that this yaw control strategy increases the impact of fatigue loads on the individual turbines, which may shorten their lifespan. Fortunately, this strategy should not often be used, according to data recorded on the Belgian grid, which will keep the damage to the WT components minimal.

AUTHOR CONTRIBUTIONS

Y. Oudich carried out the work and wrote the article, under the supervision of M. Kinnaert, F. De Belie, and J. Gyselinck.

ACKNOWLEDGEMENTS

This research is supported by the Belgian PhairywinD project,[22] funded by the Belgian Energy Transition Fund (FPS Economy).

CONFLICT OF INTEREST STATEMENT

No potential conflict of interests is declared by the authors.

PEER REVIEW

The peer review history for this article is available at https://www.webofscience.com/api/gateway/wos/peer-review/10.1002/we.2845.

DATA AVAILABILITY STATEMENT

Data supporting the results of this article can be shared by the corresponding author under reasonable request.

ORCID

Younes Oudich https://orcid.org/0000-0003-1271-816X

REFERENCES

1. Commission Regulation (EU) 2016/631. Establishing a network code on requirements for grid connection of generators. The European commission; 2016.
2. Elorza I, Calleja C, Pujana-Arrese A. On wind turbine power delta control. *Energies*. 2019;12(12):2344.
3. Wang Y, Bayem H, Giralt-Devant M, Silva V, Guillaud X, Francois B. Methods for assessing available wind primary power reserve. *IEEE Trans Sustain Energy*. 2015;6(1):272-280.
4. Aho J, Pao L, Fleming P. An active power control system for wind turbines capable of primary and secondary frequency control for supporting grid reliability. In: 51st AIAA Aerospace Sciences Meeting including the New Horizons Forum and Aerospace Exposition; 2013.
5. OpenFAST Documentation. NREL. 2022. Accessed January 03, 2023. http://openfast.readthedocs.io/
6. Van der Hoek D, Kanev S, Engels W. Comparison of down-regulation strategies for wind farm control and their effects on fatigue loads. In: 2018 American Control Conference (ACC); 2018:3116-3121.
7. Deshpande A, Peters R. Wind turbine controller design considerations for improved wind farm level curtailment tracking. In: 2012 IEEE Power and Energy Society General Meeting; 2012.
8. Van Wingerden J, Pao L, Aho J, Fleming P. Active power control of waked wind farms. *IFAC-PapersOnLine*. 2017;50(1):4484-4491.
9. Fleming P, Gebraad P, Lee S, et al. Evaluating techniques for redirecting turbine wakes using SOWFA. *Renew Energy*. 2014;70:211-218.
10. Kheirabadi A, Nagamune R. A quantitative review of wind farm control with the objective of wind farm power maximization. *J Wind Eng Ind Aerodyn*. 2019;192:45-73.
11. Fleming P, Gebraad P, Churchfield M, et al. SOWFA + super controller user's manual. National Renewable Energy Laboratory (U.S.). NREL; 2013.
12. Annoni J, Seiler P, Johnson K, Fleming P, Gebraad P. Evaluating wake models for wind farm control. In: 2014 American Control Conference; 2014: 2517-2523.
13. Brusca S, Lanzafame R, Famoso F, Galvagno A, Messina M, Mauro S, Prestipino M. On the wind turbine wake mathematical modelling. *Energy Procedia*. 2018;148:202-209.
14. Katic I, Højstrup J, Jensen NO. A simple model for cluster efficiency. *EWEC'86. Proceedings*, Vol. 1: A. Raguzzi, Rome, European Wind Energy Association Conference and Exhibition; 1987:407-410.
15. Jensen NO. A note on wind generator interaction. In: Risø National Laboratory. Risø,-M, Vol. 2411; 1983.
16. Vermeulen P, Builtjes P, Dekker J, Van Bueren GL. An experimental study of the wake behind a full scale vertical-axis wind turbine. *TNO-report*. 79-06118, Laan van Westenenk; 1979.
17. Park J, Law K. Layout optimization for maximizing wind farm power production using sequential convex programming. *Appl Energy*. 2015;151: 320-334.
18. Park J, Law K. Cooperative wind turbine control for maximizing wind farm power using sequential convex programming. *Energy Convers Manag*. 2015; 101:295-316.

10991824, 2023, 8, Downloaded from https://onlinelibrary.wiley.com/doi/10.1002/we.2845 by EVIDENCE AID - BELGIUM, Wiley Online Library on [03/10/2023]. See the Terms and Conditions (https://onlinelibrary.wiley.com/terms-and-conditions) on Wiley Online Library for rules of use; OA articles are governed by the applicable Creative Commons License

19. Gionfra N, Sandou G, Siguerdidjane H, Faille D, Loevenbruck P. Wind farm distributed PSO-based control for constrained power generation maximization. *Renew Energy*. 2019;133:103-117.
20. Gebraad P, Teeuwisse F, Van Wingerden J, Fleming P, Ruben S, Marden J, Pao L. Wind plant power optimization through yaw control using a parametric model for wake effects-a CFD simulation study. *Wind Energy*. 2014;19(1):95-114.
21. Ovidio F. 2021. Accessed January 3, 2023. <https://odnature.naturalsciences.be/mumm/en/windfarms/project/5
22. Phairywin D. 2022. Accessed January 3, 2023. https://www.phairywind.be/
23. Elia FCR. 2018. Accessed January 3, 2023. https://www.elia.be/en/electricity-market-and-system/system-services/keeping-the-balance/fcr
24. Elia FRR. 2017. Accessed January 3, 2023. https://www.elia.be/en/electricity-market-and-system/system-services/keeping-the-balance/afrr
25. Windvision E. Enercon and Eneco. Delivery of downward aFRR by wind farms; 2015.
26. Liew J, Urban AM, Andersen SJ. Analytical model for the power-yaw sensitivity of wind turbines operating in full wake. *Wind Energy Sci*. 2020;5(1):427-437.
27. Vermeer L, Sørensen J, Crespo A. Wind turbine wake aerodynamics. *Progress Aerosp Sci*. 2003;39(6-7):467-510.
28. Ivanell S, Nilsson K, Eriksson O. Wind turbine wakes and wind farm wakes. Energiforsk; 2018.
29. Jonkman J, Butterfield S, Musial W, Scott G. Definition of a 5-MW reference wind turbine for offshore system development; 2009.
30. Jonkman J. FAST.farm user's guide and theory manual. NREL; 2021.
31. Doubrawa P, Annoni J, Jonkman J. Optimization-based calibration of FAST.Farm parameters against SOWFA. Wind Energy Symposium; 2018.
32. Jonkman J, Doubrawa P, Hamilton N, Annoni J, Fleming P. Validation of FAST.Farm against large-eddy simulations. *J Phys Conf Ser*. 2018;1037:62005.
33. MathWorks. Find minimum of constrained nonlinear multivariable function. 2021. Accessed January 3, 2023. https://nl.mathworks.com/help/optim/ug/fmincon.html
34. Pena A, Rethore P, Laan M. On the application of the Jensen wake model using a turbulence-dependent wake decay coefficient: the Sexbierum case. *Wind Energy*. 2015;19(4):763-776.
35. Kuo J, Pan K, Li N, Shen H. Wind farm yaw optimization via random search algorithm. *Energies*. 2020;13(4):865.
36. Annoni J, Bay C, Taylor T, Pao L, Fleming P, Johnson K. Efficient optimization of large wind farms for real-time control. In: American Control Conference (ACC); 2018.
37. Fleming PA, Stanley AP, Bay CJ, King J, Simley E, Doekemeijer BM, Mudafort R. Serial-refine method for fast wake-steering yaw optimization. In: Journal of Physics: Conference Series, Vol. 2265; 2022:32109.
38. Gasch R, Twele J. *Wind power plants fundamentals, design construction and operation*. New York: Springer; 2012.
39. Copernicus Climate Data Store. 2021. Accessed January 3, 2023. https://cds.climate.copernicus.eu/
40. Türk M, Emeis S. The dependence of offshore turbulence intensity on wind speed. *J Wind Eng Ind Aerodyn*. 2010;98(8-9):466-471.
41. Kim M, Dalhoff P. Yaw systems for wind turbines—overview of concepts, current challenges and design methods. *J Phys Conf Ser*. 2014;524:12086.
42. Hayman GJ. MLife theory manual for version 1.00l. NREL; 2012.
43. Elia. Frequency and FCR demand per 10 seconds. Elia Open Data Portal. Accessed February 13, 2023; 2023.

How to cite this article: Oudich Y, Gyselinck J, De Belie F, Kinnaert M. Providing power reserve for secondary grid frequency regulation of offshore wind farms through yaw control. *Wind Energy*. 2023;26(8):850-873. doi:10.1002/we.2845

10991824, 2023, 8, Downloaded from https://onlinelibrary.wiley.com/doi/10.1002/we.2845 by EVIDENCE AID - BELGIUM, Wiley Online Library on [03/10/2023]. See the Terms and Conditions (https://onlinelibrary.wiley.com/terms-and-conditions) on Wiley Online Library for rules of use; OA articles are governed by the applicable Creative Commons License